The tectonic transition from oceanic subduction to continental subduction: Zirconological constraints from two types of...

Article *in* Lithos · February 2016

DOI: 10.1016/j.lithos.2015.12.003

7 authors, including:

Ren-Xu Chen
University of Science and Technology of China

Yong-Fei Zheng
University of Science and Technology of China

Zhaochu Hu
China University of Geosciences

Yueheng Yang
Chinese Academy of Sciences

Lithos 244 (2016) 122–139

Contents lists available at ScienceDirect

Lithos

journal homepage: www.elsevier.com/locate/lithos

The tectonic transition from oceanic subduction to continental subduction: Zirconological constraints from two types of eclogites in the North Qaidam orogen, northern Tibet

Long Zhang [a], Ren-Xu Chen [a,*], Yong-Fei Zheng [a], Wan-Cai Li [a], Zhaochu Hu [b], Yueheng Yang [c], Haolan Tang [d]

[a] CAS Key Laboratory of Crust–Mantle Materials and Environments, School of Earth and Space Sciences, University of Science and Technology of China, Hefei 230026, China
[b] State Key Laboratory of Geological Processes and Mineral Resources, Faculty of Earth Sciences, China University of Geosciences, Wuhan 430074, China
[c] State Key Laboratory of Lithospheric Evolution, Institute of Geology and Geophysics, Beijing 100029, China
[d] Department of Earth and Space Sciences, University of California, Los Angeles, CA 90095, USA

ARTICLE INFO

Article history:
Received 18 July 2015
Accepted 11 December 2015
Available online 19 December 2015

Keywords:
North Qaidam
Zircon
Eclogite
Oceanic subduction
Continental subduction

ABSTRACT

In the plate tectonics theory, continental subduction is pulled by subduction of dense oceanic crust. In practice, however, it is not easy to demonstrate that preceding oceanic crust exposes as oceanic-type eclogite together with continental-type eclogite in collisional orogens. The North Qaidam orogen in northern Tibet is an ultrahigh-pressure (UHP) metamorphic belt that contains the two types of eclogites, providing us with an excellent opportunity to study the tectonic transition from oceanic subduction to continental subduction. In order to constrain the protolith nature and metamorphic evolution of eclogites, we performed a combined study of zircon U–Pb ages, trace elements, mineral inclusions and O–Hf isotopes for various eclogites from the orogen. We discriminate the two types of eclogites by their differences in zircon U–Pb ages and O–Hf isotopes. CL-dark zircon domains exhibit high Th/U ratios, steep HREE patterns and significantly negative Eu anomalies, indicating that they are protolith zircons of magmatic origin with different extents of metamorphic recrystallization. Relict magmatic zircon domains in Type I eclogites yield Neoproterozoic protolith ages of >830 Ma and Hf model ages of 850–1100 Ma, whereas those in Type II eclogites yield Cambrian protolith U–Pb ages of >489 Ma and Hf model ages of 500–650 Ma. Most of the CL-bright zircon domains show low Th/U ratios, flat HREE patterns and no negative Eu anomalies, and contain mineral inclusions of garnet, omphacite and rutile, indicating their growth under eclogite-facies metamorphic conditions. These metamorphic domains have consistent eclogite-facies metamorphic ages of 433–440 Ma throughout the North Qaidam orogen, regardless of the eclogite types and locations. The metamorphic zircon domains in Type I eclogites mostly exhibit $\delta^{18}O$ values higher than normal mantle values, whereas Type II eclogites mostly have $\delta^{18}O$ values lower than the normal mantle values. The difference in the $\delta^{18}O$ values indicates that their protoliths underwent different temperatures of hydrothermal alteration at different tectonic settings. Combining zircon U–Pb ages and O–Hf isotope compositions with local tectonics, it is inferred that Type I eclogites were metamorphosed from Neoproterozoic continental mafic rocks, whereas Type II eclogites were metamorphosed from oceanic mafic rocks that were subducted prior to the continental subduction. The consistent eclogite-facies metamorphic ages for the two types of eclogites indicate that the exhumed oceanic-type eclogite was detached from the subducted oceanic crust and then entrained by the exhuming continental crust. Therefore, the coexistence of oceanic- and continental-type eclogites in the North Qaidam orogen demonstrates the tectonic transition from oceanic subduction to continental collision in the early Paleozoic.

1. Introduction

Since the findings of coesite and diamond in supracrustal rocks of metamorphic origin (Chopin, 1984; Smith, 1984; Sobolev and Shatsky, 1990; Xu et al., 1992), it is well established that low-density continental crust is subductable to mantle depths, transformed into ultrahigh-pressure (UHP) metamorphic rocks, and then exhumed to the surface (Chopin, 2003; Gilotti, 2013; Zheng, 2012). As the continental crust is too low in density to sink into the mantle, it is generally held that preceding subduction of dense oceanic slab drives subduction of the attached continental slab to mantle depths subsequent to the closure of oceanic basins (Davies and von Blanckenburg, 1995; O'Brien, 2001). After breakoff between the oceanic and continental slabs, the buoyancy force of continental crust leads to its exhumation along the subduction channel to shallow levels (Davies and von Blanckenburg, 1995; Ernst et al., 1997; Guillot et al., 2009; Zheng et al., 2013a). Thus continental collision zones containing high-pressure (HP) to UHP metamorphic

* Corresponding author.
E-mail address: chenrx@ustc.edu.cn (R.-X. Chen).

http://dx.doi.org/10.1016/j.lithos.2015.12.003
0024-4937/

rocks would have experienced the tectonic evolution from oceanic subduction to continental subduction (e.g., O'Brien, 2001; Song et al., 2006, 2014; Zheng et al., 2015).

In some HP–UHP metamorphic zones, the subducted oceanic crust was also exhumed together with the subducted continental crust to the surface. This is illustrated in the western Alps orogen of western Europe (Compagnoni and Rolfo, 2003) and the Hong'an orogen of east-central China (Wu and Zheng, 2013; Wu et al., 2009; Zhou et al., 2015). The concomitant outcrops of HP–UHP metamorphic rocks with protoliths of both oceanic and continental origins allow the bulk processes of crustal subduction and collisonal orogenesis to be restored (Beltrando et al., 2010; Wu and Zheng, 2013; Wu et al., 2009; Zhou et al., 2015). Knowledge about the consumption of oceanic crust and the subduction of continental crust as well as their transition depends on the correct recognition and distinction between oceanic and continental units in the same HP–UHP metamorphic zones. Eclogite is a common lithology in HP–UHP zones and it may be metamorphosed from mafic rocks of continental and oceanic origins, respectively, corresponding to continental-type and oceanic-type eclogites. Information about previously subducted protolith and HP–UHP metamorphism can be well preserved in eclogites compared to other lithologies. Therefore, the protolith nature and age of eclogites are pivotal not only in deciphering the spatial-temporal distributions of oceanic and continental units but also in revealing the tectonic transition from oceanic subduction to continental subduction (Rubatto et al., 1998; Wu and Zheng, 2013; Wu et al., 2009; Zhou et al., 2015).

Zircon is a robust mineral that has been widely used for U–Pb dating and geochemical tracing (Chen et al., 2010; Hanchar and Hoskin, 2003; Harley and Kelly, 2007; Hawkesworth and Kemp, 2006; Scherer et al., 2007). In deeply subducted crustal rocks, the mineral inclusions, trace element composition and O–Hf isotopes of relict and metamorphic zircon domains have been used to constrain the protolith and metamorphic ages, protolith nature and metamorphic conditions (Chen et al., 2011; Liu and Liou, 2011; Rubatto and Hermann, 2003, 2007; Zheng et al., 2005, 2006). In HP–UHP metamorphic zones with concomitant outcrops of oceanic- and continental-type eclogites, the mafic protoliths of oceanic- and continental-type eclogites may be extracted from depleted or enriched mantle sources at different ages. While the mafic protolith of oceanic origin would be present for a short timescale before subduction, the mafic protolith of continental origin would be present for a long timescale before subduction (Zheng, 2012). Thus relict magmatic zircon domains can be used to determine protolith U–Pb ages and geochemical compositions. The difference in the residence time and subduction history of mafic protoliths also leads to the differences in the U–Pb ages and O–Hf isotopes of metamorphic zircon in eclogites. Therefore, both the relict magmatic and metamorphic zircon in eclogites are not only crucial in revealing the protolith nature of various eclogites, but also vital in constraining the timescale of orogenic evolution.

The North Qaidam orogen, located in the northeastern edge of Tibetan Plateau, is an early Paleozoic collisional orogen with the characteristic occurrence of continental-type eclogites (Song et al., 2006, 2014; Zhang et al., 2008, 2013a). The occurrence of oceanic-type eclogites was also suggested, but it has been debated whether the fossil oceanic unit did exist (Yu et al., 2013; Zhang et al., 2010). This is primarily related to the distribution and age of possible oceanic-type eclogites in this orogen (Mattinson et al., 2006; Song et al., 2006, 2014; Zhang et al., 2008, 2013a). If it is true, this orogen is an excellent candidate to study the distinction between oceanic- and continental-type eclogites and the tectonic transition from oceanic subduction to continental subduction. This paper presents an integrated study of zircon U–Pb ages, trace elements, mineral inclusions and O–Hf isotopes for eclogites from the North Qaidam orogen. The results provide insights into the protolith nature and metamorphic evolution of eclogites. Furthermore, the geochronological evolution of oceanic- and continental-type eclogites is also constrained with respect to the tectonic transition from oceanic subduction to continental subduction in the early Paleozoic.

2. Geological setting and samples

The North Qaidam orogen extends in a NW–SE direction between the Qaidam Block to the south and the Qilian Block to the north for about 400 km, and is located in the northeastern margin of Tibetan Plateau (Fig. 1). It is truncated by the Wenquan Fault in the southeast and the giant Altyn Tagh Fault in the northwest. It is a typical Alpine-type UHP metamorphic zone due to the early Paleozoic subduction of the Qaidam Block beneath the Qilian Block (e.g., Liou et al., 2009; Song et al., 2014). There are four subunits exposing UHP metamorphic rocks from southeast to northwest (Fig. 1): the Dulan eclogite-gneiss terrane, the Xitieshan eclogite-gneiss terrane, the Lüliangshan peridotite-gneiss terrane and the Yuka eclogite-gneiss terrane. Metamorphic lithologies are dominated by granitic and pelitic gneisses, with eclogites occurring as interlayers and lenses in the gneisses in the Dulan, Xitieshan and Yuka terranes. Coesite inclusions have been found in zircon and garnet from metapelites and eclogites (Liu et al., 2012a; Song et al., 2003; Yang et al., 2002; Yu et al., 2013; Zhang et al., 2009a, 2009b, 2010). Diamond inclusions in zircon and garnet exsolution structures have also been observed in peridotite from the Lüliangshan terrane (Song et al., 2004, 2005a, 2005b). These observations indicate the subduction of continental crust to a mantle depth greater than 200 km for UHP metamorphism. The UHP metamorphic rocks are in fault contact with volcanic and sedimentary rocks of the Tanjianshan group. The basaltic rocks of the Tanjianshan group, with eruption ages of 468–534 Ma, are considered to be island arc volcanics or obducted ophiolitic rocks (Shi et al., 2006; Zhu et al., 2015). The UHP metamorphic rocks are also widely intruded by granitic intrusions with variable ages ranging from Ordovician to Permian (e.g., Song et al., 2014).

Earlier studies claimed that all the eclogites from the North Qaidam orogen are derived from subducted oceanic crust, based on their partial similarity in trace element patterns and positive $\varepsilon_{Nd}(t)$ values to mid-ocean ridge basalts (Song et al., 2006; Yang et al., 2006). However, later studies have demonstrated that the majority of eclogites have geochemical features similar to continental rift or flood basalts with >800 Ma protolith ages and 420–460 Ma eclogite-facies metamorphic ages (Song et al., 2014, and references therein). Thus these eclogites are suggested to derive from metamorphism of continental basalts. However, two cross sections from the Yematan and Shaliuhe area in the Dulan terrane with the outcrops of ultramafics and eclogites, sharing some geochemical characteristics with oceanic lithosphere, are suggested to be metamorphosed ophiolite-like sequence (Song et al., 2014; Zhang et al., 2008, 2009a, 2013a). Zircon U–Pb dating for a kyanite eclogite from the Shaliuhe section yields Cambrian protolith ages, in contrast to the Neoproterozoic protolith ages for continental-type eclogites elsewhere (Song et al., 2003, 2006; Zhang et al., 2008, 2009a, 2013a). However, the interpretation of eclogite geochemistry is versatile and the few discordant Cambrian U–Pb ages with large errors may result from metamorphic resetting. Therefore, it is still debated whether the oceanic-type eclogites do exist (Yu et al., 2013; Zhang et al., 2010). Furthermore, if the oceanic-type eclogites are indeed present, their distribution, metamorphic evolution and protolith nature are still not well constrained. On the other hand, the interpretation for the large range of eclogite-facies metamorphic ages is debated. The protracted metamorphic ages are explained to result from either multiple metamorphic episodes during the transition from oceanic subduction to continental collision (Song et al., 2014), or prolonged metamorphism in the large UHP terrane (Mattinson et al., 2006). The correct interpretation of metamorphic ages for the different types of eclogites is critical to the tectonic transition from oceanic subduction to continental collision.

This study deals with eclogites and their retrograde counterparts, which were collected from all three subunits that expose eclogites in

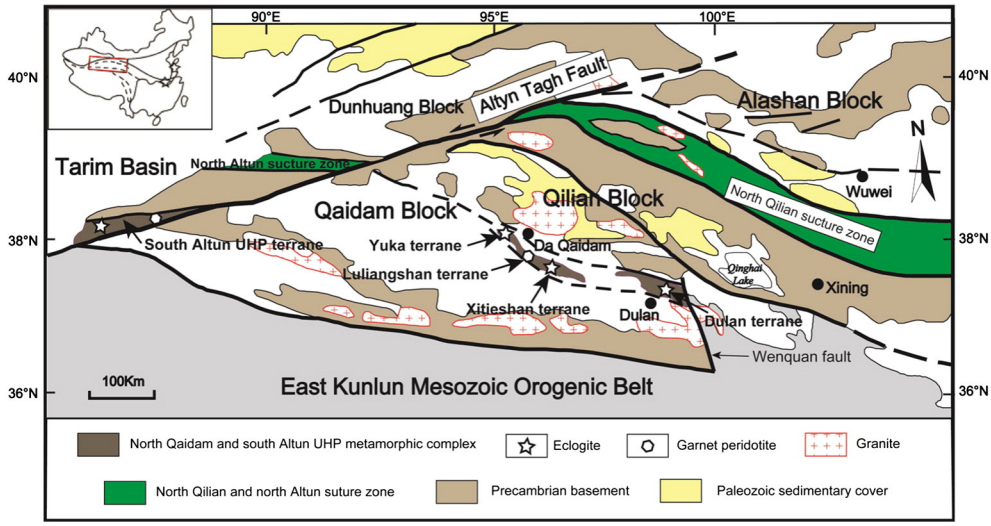

Fig. 1. Simplified map of geology for the North Qaidam orogen and adjacent areas in northern Tibet (revised after Song et al., 2006).

the North Qaidam orogen. They include two garnet amphibolites 09QL86 and 09QL93 from the Xitieshan terrane, one fresh eclogite 09QL105 from the Yuka terrane, one kyanite eclogite 13NQ02 and one garnet amphibolite 09QL32 from the Shaliuhe area of the Dulan terrane, and one fresh bimineral eclogite 13NQ38 and two garnet amphibolites 13NQ44 and 13NQ52 from the Yematan area of the Dulan terrane.

3. Analytical methods

Representative zircon grains were separated from crushed samples and embedded in epoxy resin and polished down to half sections. Before microbeam analyses, CL images of zircon grains were obtained using a MIRA3 TESCAN scanning electron microscope at CAS Key Laboratory of Crust–Mantle Materials and Environments in University of Science and Technology of China (USTC). The internal structures revealed by CL are used as guide for microbeam analyses. Mineral inclusions in zircon were identified by a ThermoFisher DXR Laser Raman Spectrometer at the same laboratory.

3.1. SIMS analysis of zircon U–Pb ages and O isotopes

The measurements of zircon O isotopes were conducted on a Cameca IMS1280 secondary ion mass spectrometer (SIMS) at State Key Laboratory of Lithospheric Evolution in Institute of Geology and Geophysics in Chinese Academy of Sciences (CAS), Beijing and on a Cameca IMS1270 SIMS in University of California at Los Angeles, USA. Instrumental conditions and data treatments at both labs were as described by Li et al. (2010a) and Trail et al. (2007), respectively. The primary Cs^+ beam has a diameter of about 20 μm. Measured $^{18}O/^{16}O$ ratios were normalized using VSMOW ($^{18}O/^{16}O = 0.0020052$) and reported in the conventional $\delta^{18}O$ notation in the unit of permil. Instrumental mass fractionation was corrected using zircon standard Penglai with a recommended $\delta^{18}O$ value of 5.31 ± 0.1‰ (Li et al., 2010b). Zircon standard Qinghu with a recommended $\delta^{18}O$ value of 5.4 ± 0.2‰ was also analyzed to monitor data quality (Li et al., 2013). The internal precision of a single analysis is generally better than ± 0.2‰ for $\delta^{18}O$ values.

After the O isotope analysis, the mounted zircons were carefully repolished and then used for the U–Pb dating by the Cameca IMS1280 ion microprobe at Institute of Geology and Geophysics in CAS, Beijing. The analytical procedures are described in detail by Li et al. (2010a). An O_2^- primary beam, about 20 × 30 μm in size, was targeted directly onto the same domains of the O isotope analysis. By this way, the SIMS zircon U–Pb age could be correlated with O isotope. Zircon ages for samples are calibrated against the 337 Ma zircon standard Plešovice (Sláma et al., 2008). Common Pb was corrected by measuring ^{204}Pb directly. Analytical errors for the $^{206}Pb/^{238}U$ age of Plešovice zircon are generally better than ± 0.7–0.8%. Zircon standard Qinghu was also measured to monitor instrumental drift. ISOPLOT program was used to calculate apparent U–Pb ages and plot U–Pb concordia diagrams (Ludwig, 2003).

3.2. LA-ICP-MS analysis of zircon U–Pb ages and trace elements

After the SIMS analyses, the zircon samples were re-polished for the laser analyses. Zircon U–Pb dating and trace element analyses were performed using an Agilent 7500a ICP-MS coupled with a 193 nm ArF-excimer laser-ablation system (GeoLas 2005) at State Key Laboratory of Geological Processes and Mineral Resources in China University of Geosciences, Wuhan. The instrumental conditions and data acquisition methods were described by Liu et al. (2008a, 2010). Laser beam was targeted to the same domains of the SIMS analyses when possible. The laser beam has a diameter of 32 μm, a repetition frequency of 6 Hz and laser energy of ~60 mJ. Ablated zircon materials were transported into the ICP-MS by He, mixed with makeup gas Ar. The signal acquisition time is set to be 50 s, after a 20–30 s blank acquisition interval.

Off-line selection and integration of background and analyte signals, and time-drift correction and quantitative calibration for U–Pb dating and trace element analyses were performed by software *ICPMSDataCal* (Liu et al., 2008a, 2010). Zircon standard 91500 was used as external standard and its recommended U-Pb isotopic ratios are from Wiedenbeck et al. (1995). Uncertainty of preferred values for the external standard 91500 was propagated to the ultimate results of the samples. Zircon standard GJ-1 was used as a monitor and yielded $^{206}Pb/^{238}U$ age of 598 ± 4 Ma (n = 32), consistent with the recommended value of 599.8 ± 1.7 Ma (Jackson et al., 2004). Trace element concentrations of zircon were calibrated by using NIST610 as an external reference material and ^{29}Si as an internal standard element. Common Pb correction was carried out by using EXCEL program of ComPbCorr#_151 (Andersen, 2002). Apparent U–Pb ages and traditional concordia U–Pb diagrams were obtained by the ISOPLOT program (Ludwig, 2003).

3.3. LA-MC-ICP-MS analysis of zircon Lu–Hf isotopes

After the LA-ICP-MS analysis, zircon Hf isotope analysis was measured by a LA-MC-ICP-MS at State Key Laboratory of Lithospheric Evolution in Institute of Geology and Geophysics in CAS, Beijing. Detailed analytical procedures are following those described by Xu et al. (2004) and Wu et al. (2006a). Zircon domains that have been dated for U–Pb

ages were preferred for Hf analysis. The laser beam was set to be 44 μm in size, with an ablation frequency of 8 Hz. Isobaric interference of ^{176}Lu and ^{176}Yb on ^{176}Hf were corrected by measuring interference-free ^{175}Lu and ^{172}Yb isotopes, following the methods of Iizuka and Hirata (2005). Zircon standards Mud-tank and GJ-1 were used as standard with ^{176}Hf/^{177}Hf ratios of 0.283003 ± 0.000008 (n = 40) and 0.282014 ± 0.000009 (n = 48), respectively. They are consistent with values recommended by Woodhead and Hergt (2005) and Morel et al. (2008), respectively. There is no correlation between ^{176}Yb/^{177}Hf and ^{176}Hf/^{177}Hf ratios (Fig. A1), indicating that the Yb interference is properly corrected. Initial $\varepsilon_{Hf}(t)$ values at protolith ages are calculated with reference to the chondritic reservoir suggested by Bouvier et al. (2008) adopting the decay constant of Scherer et al. (2001). Single-stage Hf model ages (T_{DM1}) are calculated relative to the depleted mantle with present-day ^{176}Hf/^{177}Hf ratio of 0.28325 and ^{176}Lu/^{177}Hf ratio of 0.0384 (Griffin et al., 2000).

4. Results

Detailed analytical results are listed in Appendix Tables A1 to A4, and a summary of the data is presented in Table 1. The SIMS and LA-ICP-MS analyses were mostly made on the same zircon domains, generally yielding similar U–Pb ages. But large differences may be present in inhomogeneous zircon such as samples 09QL93 and 09QL105, as the two methods target zircon materials from different depths. As the SIMS analyses have better precision and accuracy, the ages determined by SIMS are used for discussion. Although no correlation diagram between data measured by the various analytical methods is plotted, a full view of different zircon domains can be obtained by statistics.

4.1. Garnet amphibolite 09QL86 at Xitieshan

Zircon grains mostly show core–mantle–rim structures in the CL images (Fig. 2a). However, the cores are absent in some grains and the rims are too thin to allow the isotopic analysis. Garnet, omphacite, rutile and quartz inclusions were observed in the core and mantle domains (Fig. 3a, b). The core and mantle domains have consistent U–Pb ages with a weighted mean ^{206}Pb/^{238}U age of 437 ± 4 Ma (Fig. 4a, excluding two younger ages). All the zircon domains exhibit Th/U ratios < 0.1, flat HREE patterns without Eu anomalies (Figs. 5a and 6a), and homogeneous δ^{18}O values of 5.9–6.3‰ (Fig. 7a). Their Hf isotope compositions are uniform with ε_{Hf}(t = 830 Ma) values of 13.9–15.8 and T_{DM1} ages of 763–867 Ma (Fig. 7b).

4.2. Garnet amphibolite 09QL93 at Xitieshan

Zircon grains have CL-dark cores and CL-bright rims. Some of them occur as CL-bright grains without cores (Fig. 2b). The cores are irregularly dissolved and replaced by penetrating or isolated CL-bright domains to variable extents. In the extreme case, the CL-dark domains form a cluster of isolated islands. Quartz and plagioclase inclusions were observed in the cores (Fig. 3c), whereas garnet, quartz, rutile and omphacite inclusions were observed in the CL-bright domains. All the zircon domains yield a discordia line in the U–Pb concordia diagram, with upper and lower intercept ages of 825 ± 210 Ma and 397 ± 72 Ma, respectively (Fig. 4b). Several spots show large errors in ^{207}Pb/^{235}U ages due to high contents of common Pb. Most domains have steep HREE patterns with negative Eu anomalies (Fig. 6b). But several CL-bright domains have lower Th, U, Nb, Ta and HREE contents and lower Th/U ratios, but higher Hf contents than the cores (Fig. 5a, b, c). Besides, they have flat HREE patterns without negative Eu anomalies (Fig. 6b). The cores have δ^{18}O values of 5.0–6.6‰, whereas the CL-bright rims or grains have δ^{18}O values of 5.2–6.3‰ (Fig. 7a). The cores have ε_{Hf}(t = 830 Ma) values of 11.1-17.3 and T_{DM1} ages of 696–954 Ma, whereas the rims have slightly more radiogenic Hf isotope values than the cores (Fig. 7b).

4.3. Eclogite 09QL105 at Yuka

Zircon grains can be subdivided into CL-dark and CL-bright domains, with the former occurring as cores or grains whereas the latter occurring as rims or rare grains (Fig. 2c). Some cores show similar replacement structure to those in sample 09QL93. Quartz and muscovite inclusions were observed in the CL-dark domains, whereas garnet, omphacite and quartz inclusions were observed in the CL-bright rims (Fig. 3d). Discordant U–Pb ages are obtained from the SIMS analyses, with the CL-dark domains (^{206}Pb/^{238}U ages = 478–819 Ma) close to the upper intercept age of 868 ± 42 Ma, whereas the CL-bright domains (^{206}Pb/^{238}U ages = 417–556 Ma) close to the lower intercept age of 411 ± 84 Ma (Fig. 4c). Most of the zircon domains exhibit steep HREE patterns with negative Eu anomalies (Fig. 6c). But several rims have lowered Th, U, Nb, Ta and HREE contents and elevated Hf contents than the cores (Fig. 5a, b, c), and significantly flattened HREE patterns and weakened negative Eu anomalies (Fig. 6c). Both the CL-dark and CL-bright domains have homogeneous δ^{18}O values ranging from 4.8 to 5.9‰ (Fig. 7a). Nine cores have ε_{Hf}(t = 830 Ma) values of 8.6–13.8 and T_{DM1} ages of 841–1059 Ma (Fig. 7b).

4.4. Garnet amphibolite 13NQ44 at Yematan

Zircon grains consist of CL-dark cores and CL-bright rims, and few of them occur as homogeneous CL-bright grains (Fig. 2d). The cores have discordant ages ranging from 538 to 832 Ma, while the CL-bright domains have consistent U–Pb ages with a weighted mean of 435 ± 4 Ma (Fig. 4d). The cores have REE patterns typical of magmatic zircon, high Th, U (generally > 100 ppm), Nb and Ta contents and high Th/U ratios (generally > 1), while the CL-bright domains have flat HREE patterns without Eu anomalies, much lower contents of Th, U, Nb and Ta, higher Hf content and lower Th/U ratios (<0.1) (Figs. 5a, b, c and 6d). The cores have δ^{18}O values of 5.1–7.4‰, ε_{Hf}(t = 830 Ma) values of 7.3–13.3 and T_{DM1} ages of 860–1102 Ma (Fig. 7a, b). In contrast, the CL-bright domains have elevated δ^{18}O values of 6.3–7.7‰, elevated ε_{Hf}(t = 830 Ma) values of 13.5–23.3 and lowered T_{DM1} ages of 470–854 Ma (Fig. 7a, b).

4.5. Garnet amphibolite 09QL32 at Shaliuhe

Most zircon grains exhibit bright CL without zoning, a few of them show core-rim structure with CL-dark core and CL-bright rim (Fig. 2e). Rare garnet, omphacite and rutile inclusions are observed in the dated zircon domains (Fig. 3e, f). The SIMS analyses on these zircon domains yields coherent U–Pb ages with a weighted mean of 438 ± 3 Ma (Fig. 4e, excluding two grains with core–rim structure). All the zircon domains have similar steep HREE patterns without Eu anomalies (Fig. 6e), homogeneous δ^{18}O values of 4.8–5.9‰ (Fig. 7c), ε_{Hf}(t = 516 Ma) values of 9.8 to 14.5 and T_{DM1} ages of 540 to 730 Ma (Fig. 7d).

4.6. Kyanite eclogite 13NQ02 at Shaliuhe

Most zircon grains are CL-bright without zoning, a few grains have CL-dark cores and CL-bright rims (Fig. 2f). Rare garnet, omphacite, rutile and quartz inclusions were observed in the CL-bright domains. The CL-dark cores exhibit high Th and U contents (hundreds of ppm), high Th/U ratios (mostly > 1), and steep HREE patterns with significant negative Eu anomalies (Fig. 6f), yielding ^{206}Pb/^{238}U ages ranging from 446 to 489 Ma (Fig. 4f). The CL-bright grains have low Th (<1 ppm), U (<20 ppm), Nb and Ta contents, high Hf contents, low Th/U ratios of <0.1 (Fig. 5d, e, f), and flat HREE patterns without negative Eu anomalies (Fig. 6f), yielding a weighted mean U–Pb age of 440 ± 5 Ma (Fig. 4f). The cores and CL-bright domains have similar δ^{18}O values of 3.7 to 5.0‰ (Fig. 7c), lower than normal mantle values of 5.3 ± 0.3‰ (Valley et al., 1998). The cores have ε_{Hf}(t = 516 Ma) values of 17.5–23.0 and T_{DM1} ages of 174–

Table 1
A summary of zircon U–Pb ages, O–Hf isotopes and trace elements for metabasites from the North Qaidam orogen.

	SIMS analyses			LA-(MC)-ICP-MS analyses								
Spot	Th/U	$^{206}Pb/^{238}U$ age (Ma)	$\delta^{18}O$ (‰)	Th (ppm)	U (ppm)	Th/U	$^{206}Pb/^{238}U$ age (Ma)	$(Yb/Gd)_N$	Eu/Eu*	$^{176}Lu/^{177}Hf$	$\varepsilon_{Hf}(t)$	T_{DM1} (Ma)
Xitieshan												
09QL86 garnet amphibolite												
1	0.01	437.6 ± 6.9	6.1	0.23	9.6	0.02	448 ± 20	1.1	1.1	0.000002	15.8	763
2	0.03	419.4 ± 6.1	6.3	0.49	20.7	0.02	418 ± 19	0.8	1.5			
3	0.06	437.1 ± 6.3	6.2	1.86	20.9	0.09	438 ± 16	1.7	0.8	0.000009	14.7	805
4	0.02	440.1 ± 6.8	6.3	1.13	16.6	0.07	441 ± 21	1.4	1.8	0.000012	14.6	809
5	0.01	435.4 ± 6.4	6.2									
6	0.03	424.3 ± 6.3	6.2									
7	0.03	433.3 ± 6.3	5.9							0.000014	15.1	788
8	0.01	432.7 ± 6.4	6.1	0.33	42.2	0.01	433 ± 14	1.4	0.8	0.000011	14.2	823
9	0.02	427.8 ± 6.4	6.2							0.000016	13.9	837
11	0.01	446.4 ± 6.5	6.2	0.43	39.7	0.01	449 ± 14	0.9	1.1			
12	0.05	451.8 ± 6.6	6.3	0.70	45.7	0.02	453 ± 15	1.3	1.6	0.000018	14.9	796
13	0.05	408.0 ± 6.0	5.9							0.000015	14.0	832
14	0.01	448.1 ± 6.6	6.1	0.94	64.4	0.01	449 ± 14	1.0	0.8	0.000005	15.3	780
16	0.01	430.8 ± 6.3	6.3									
17	0.01	435.3 ± 6.3	6.0	0.26	21.1	0.01	437 ± 18	0.9	2.4	0.000008	14.5	814
18	0.01	441.4 ± 6.9	6.2	0.44	51.0	0.01	447 ± 14	0.6	0.9	0.000010	15.4	778
19	0.02	445.1 ± 6.5	5.9	1.19	49.4	0.02	445 ± 15	1.0	1.4	0.000010	14.5	815
20	0.02	430.6 ± 6.4	5.9	1.03	54.6	0.02	447 ± 12	1.0	0.7	0.000013	14.8	803
09QL93 garnet amphibolite												
1c			5.2	289	2268	0.13	625 + 9	98.1	0.3	0.001845	15.5	772
3c	1.49	438.0 + 6.5	5.0	688	1089	0.63	507 + 7	63.3	0.6	0.003436	13.1	872
4	0.16	407.8 + 5.9	5.9	41	255	0.16	492 + 10	58.4	0.3	0.000498	13.8	838
6	0.65	516.1 + 7.4	6.4	57	155	0.37	601 + 14	18.9	0.5	0.003859	13.4	858
7c	0.53	516.8 + 7.5	5.8	105	254	0.41	561 + 10	26.4	0.2	0.001849	14.2	826
8c	0.53	490.8 + 7.3	6.2	133	374	0.36	677 + 10	4.5	0.1	0.002941	13.5	854
9	2.98	579.1 + 8.3	6.2							0.001190	18.4	655
10			6.0									
11c	0.16	436.6 + 6.3	6.6	158	531	0.30	571 + 10	42.4	0.1	0.002352	11.1	954
12	0.02	424.5 + 6.3	6.1	0.55	6.9	0.08		77.7	0.9	0.000061	16.3	742
14	1.03	435.6 + 6.3	5.9									
15			6.2									
16c			6.2	561	499	1.13	490 + 12	31.9	0.4	0.001893	16.3	738
17			5.9	1.48	7.8	0.19		3.7				
18	0.05	432.4 + 6.3	6.3	3.04	45	0.07		1.6	1.3	0.000006	17.3	703
19	0.16	670.1 + 9.6	5.5	3.35	18.4	0.18		10.6	4.2			
21c	0.23	431.2 + 7.4	6.0	76	352	0.22	539 + 16	53.7	1.7	0.001844	17.3	696
22	0.16	411.8 + 6.0	5.6		396		614 + 11	7.7	0.4	0.001034	15.2	786
23			5.8	9.2	66	0.14		64.0	0.2	0.000464	21.8	524
24	1.02	570.2 + 8.3	6.2	0.20	8.5	0.02		16.2	1.3	0.000012	17.4	701
25	0.06	432.9 + 7.8	5.9	0.30	3.25	0.09		137.0	1.1			
26				290	804	0.36	466 + 7	15.4	0.1			
27					1106		449 + 8	13.7	0.6			
Yuka												
09QL105 eclogite												
1c	1.17	755.7 + 11	5.0	318	348	0.92	813 + 16	5.6	0.2	0.004024	10.6	979
2c			5.7									
3	0.29	500.3 + 7.5	5.7	533	443	1.20	829 + 12	7.8	0.1			
4c	0.87	745.3 + 10.6	4.9	532	442	1.20	803 + 11	7.5	0.2	0.002943	8.6	1059
5			4.9	4.2	6.3	0.67		13.2	0.0			
6			5.2	15.9	5.0	3.20		13.1	0.6			
7c				3600	1191	3.02	611 + 7	11.1	0.2			
8c	1.40	761 + 11.8	5.3	455	459	0.99	849 + 19	14.9	0.3	0.001545	11.0	952
9	1.99	555.8 + 14.5	5.8	1070	393	2.72	666 + 10	32.4	0.8	0.004045	13.8	841
10			5.6	307	76	4.06		13.2	1.4			
11c	1.68	818.7 + 11.6	5.3	1150	639	1.80	809 + 12	18.5	0.2	0.001709	11.0	953
12c	1.18	561.6 + 12.2	5.2							0.001802	9.7	1006
13			5.4	718	390	1.84	679 + 11	28.8	0.4			
14c	0.34	478.6 + 7	5.1		930		469 + 10	10.9	0.5			
15	0.02	417.3 + 6.1	5.3	2.66	20.3	0.13		8.9	0.2	0.003181	15.3	779
16			5.4	54	44	1.23		16.1	0.5			
17c	2.96	749 + 10.6	5.0	728	431	1.69	805 + 12	18.5	0.1	0.003020	13.7	847
18	1.14	440.9 + 7.3	5.9	398	303	1.31	724 + 12	12.6	0.2			
19c	1.57	804.7 + 11.4	5.2	1837	1150	1.60	726 + 10	9.5	0.2	0.003191	11.4	942
20c			5.9	876	684	1.28	506 + 9	17.9	0.4			
21c			4.8	947	1227	0.77	726 + 18	16.8	0.2			
22			4.9	645	519	1.24	771 + 12	10.6	0.3			
23				305	281	1.09	656 + 11	25.4	0.2			
24c				1046	862	1.21	748 + 10	7.3	0.2			

Table 1 (*continued*)

	SIMS analyses			LA-(MC)-ICP-MS analyses								
Spot	Th/U	$^{206}Pb/^{238}U$ age (Ma)	$\delta^{18}O$ (‰)	Th (ppm)	U (ppm)	Th/U	$^{206}Pb/^{238}U$ age (Ma)	$(Yb/Gd)_N$	Eu/Eu*	$^{176}Lu/^{177}Hf$	$\varepsilon_{Hf}(t)$	T_{DM1} (Ma)
Yematan in Dulan												
13NQ44												
1c	0.27	538.5 + 7.9	7.4	76.7	206.3	0.37	626 + 3	12.2	0.1	0.001526	8.7	1046
2c	1.53	783.6 + 11.1	5.1	501.7	461.0	1.09	783 + 3	8.5	0.1	0.000579	10.0	989
3c	1.39	820.9 + 11.6	5.4	799.4	490.0	1.63	826 + 4	6.6	0.1	0.002104	13.3	860
4	0.01	427.8 + 6.2	6.8	1.1	95.5	0.01	429 + 4	2.8	1.0	0.000010	23.3	470
5c	1.31	749.6 + 10.6	5.7	372.1	273.8	1.36	750 + 4	7.1	0.1	0.001221	11.5	931
6	0.01	434.6 + 6.4	7.4	1.5	114.8	0.01	435 + 4	2.1	1.2	0.000004	15.7	766
7c	1.10	716.3 + 10.2	6.2	241.8	370.8	0.65	577 + 3	7.3	0.1			
8	0.01	436.5 + 6.4	7.3	1.6	80.1	0.02	437 + 5	4.2	1.1	0.001111	13.5	854
9	0.01	427.8 + 6.2	7.7	2.7	167.5	0.02	427 + 3	2.4	1.2	0.000011	20.9	562
10c	1.22	723.2 + 10.3	6.3	522.4	432.1	1.21	731 + 3	6.5	0.1	0.001417	7.6	1088
11	0.02	432.7 + 6.3	7.5	3.8	159.9	0.02	434 + 4	2.8	0.8	0.000321	16.1	750
12c	1.49	690.3 + 9.8	6.7	242.4	184.4	1.31	689 + 5	9.6	0.1	0.001298	7.3	1102
13	0.00	445.5 + 6.5	7.7	0.6	73.3	0.01	447 + 4	1.5	1.1	0.000005	15.9	757
14	0.01	433.4 + 6.3	7.2	2.2	150.8	0.01	434 + 3	0.6	1.2	0.000005	13.8	842
15	0.02	442.8 + 6.5	6.7	2.5	156.1	0.02	443 + 4	2.4	1.3	0.000799	14.8	802
16c	1.24	705.6 + 10	6.5	529.3	439.5	1.20	707 + 4	8.0	0.1	0.001607	10.3	983
17	0.02	430.5 + 6.3	7.2	1.2	106.0	0.01	431 + 4	1.8	1.1	0.000007	22.8	490
18	0.04	442.5 + 6.4	6.3	2.2	255.4	0.01	435 + 2	2.8	1.1	0.000016	17.0	717
19c	1.27	831.6 + 11.8	5.9	70.4	75.7	0.93	831 + 6	9.2	0.1	0.001133	11.5	932
21	0.01	434.6 + 6.4	7.6	2.1	125.9	0.02	436 + 3	2.1	1.2	0.000015	16.5	733
22c	0.44	806.1 + 11.4	5.7	73.1	110.8	0.66	803 + 7	11.6	0.2	0.001187	12.6	890
23	0.01	430.8 + 6.3	6.5	1.3	107.2	0.01	432 + 3	2.6	0.9	0.000275	14.4	816
24				14.6	237.4	0.06	442 + 3	3.0	0.9	0.001852	16.0	749
Shaliuhe in Dulan												
09QL32 garnet amphibolite												
1	0.41	435.2 ± 6.4	5.9	18	33	0.54	447 ± 12	45.4	1.2	0.000366	11.3	668
2	0.41	435.6 ± 6.3	5.7									
3	0.66	445.5 ± 6.5	5.6	80	84	0.95	447 ± 8	21.9	0.8	0.001539	12.2	636
4	0.45	420.1 ± 6.2	5.4	116	112	1.03	447 ± 7	39.0	0.9	0.001457	10.4	710
7	0.37	439.3 ± 6.5	5.5	29	59	0.48	441 ± 10	44.4	0.7	0.000790	11.3	670
8	0.45	442.0 ± 6.5	5.4	23	42	0.56	449 ± 12	45.3	0.8	0.000868	9.8	730
9	0.49	438.8 ± 6.5	4.9	39	63	0.62	467 ± 12	36.2	1.7	0.000386	12.0	640
10	0.36	426.9 ± 6.2	5.5							0.000124	14.5	540
12	0.81	442.6 ± 6.4	5.0	327	274	1.19	453 ± 7	19.6	0.8	0.000981	13.7	575
14	0.37	433.6 ± 6.3	5.5	50	103	0.49	445 ± 10	54.4	2.4	0.000379	10.0	719
15	0.42	429.2 ± 6.2	4.8	27	54	0.50	437 ± 11	46.6	0.8	0.000799	10.2	712
16	0.47	438.4 ± 6.4	5.4	40	74	0.54	443 ± 10	36.4	1.1			
17	0.41	443.9 ± 6.5	5.3	69	125	0.55	439 ± 8	28.1	0.8			
18	1.07	435.8 ± 6.3	5.5							0.000424	12.1	636
19	0.41	433.5 ± 6.3	5.4	32	72	0.45	437 ± 11	62.6	1.2	0.000618	12.4	625
20	0.44	428.3 ± 6.3	5.3	41	84	0.48	453 ± 10	44.8	1.2	0.000620	12.1	635
21	0.37	432.3 ± 6.3	5.4									
22	0.35	424.8 ± 6.2	4.9									
23	0.99	454.3 ± 6.6	5.3							0.000711	13.2	592
27	0.39	441.2 ± 6.9	5.6	40	108	0.37	446 ± 10	36.2	0.7	0.000810	11.3	668
28	0.40	439.7 ± 6.4	5.1							0.000305	12.0	638
30	0.38	434.9 ± 6.3	5.1							0.000247	12.2	631
31	1.04	438.2 ± 6.4	5.0									
32	0.47	447.1 ± 6.5	4.8							0.000603	12.1	638
33	0.59	452.6 ± 6.6	4.8	73	157	0.47	453 ± 9	37.4	0.7	0.000474	14.3	551
13NQ02 kyanite eclogite												
1			4.2	0.01	7.98	0.00	425 + 12	4.6		0.000002	18.7	376
2	0.01	447.7 + 6.5	4.3	0.61	9.45	0.07	446 + 10	2.5	1.4	0.000002	15.7	493
3	0.01	434.9 + 6.4	4.4	0.62	18.58	0.03	435 + 7	1.5	1.0	0.000002	13.9	564
4			4.3									
5c	0.10	446.4 + 6.5	4.5	1350	566	2.38	448 + 2	55.1	0.2	0.004345	18.6	363
6	0.01	436.3 + 6.3	4.4	0.05	10.54	0.00	436 + 9	1.5	1.1	0.000001	16.4	467
9			3.7									
10	0.01	439.7 + 7	4.4	0.07	11.52	0.01	440 + 10	1.6	1.0	0.000004	19.1	361
11			4.6									
12			3.9									
13			3.8									
14	0.01	442.5 + 8.2	4.1	0.05	11.17	0.00	441 + 9	3.8	1.2	0.000002	14.0	561
15c	1.23	472.7 + 6.9	3.8	2008	939	2.14	473 + 2	17.8	0.2			
16			4.3									
17	0.03	437.7 + 6.4	4.5	0.15	11.34	0.01	440 + 9	1.3	1.6	0.000002	15.7	496
18c			3.8	3807	1298	2.93	461 + 2	57.3	0.1	0.003766	23.0	174
19c	2.19	489 + 7.1	4.3	6348	2523	2.52	488 + 2	18.4	0.2	0.002734	20.5	291
20c	0.42	447.4 + 6.5	5.0	517	491	1.05	448 + 3	22.4	0.1			
21c			4.4	391	499	0.78	452 + 3	44.5	0.1	0.002436	20.4	298

(*continued on next page*)

Table 1 (*continued*)

	SIMS analyses			LA-(MC)-ICP-MS analyses								
Spot	Th/U	$^{206}Pb/^{238}U$ age (Ma)	$\delta^{18}O$ (‰)	Th (ppm)	U (ppm)	Th/U	$^{206}Pb/^{238}U$ age (Ma)	$(Yb/Gd)_N$	Eu/Eu*	$^{176}Lu/^{177}Hf$	$\varepsilon_{Hf}(t)$	T_{DM1} (Ma)
22c	1.15	452.1 + 6.6	4.9	958	648	1.48	478 + 2	23.5	0.2	0.000707	22.3	231
23c				451	290	1.56	444 + 2	59.9	0.1	0.003084	17.5	415
Yematan in Dulan												
13NQ38 eclogite												
1	0.04	444 + 6.5	5.2	1.7	50.3	0.03	445 + 6	1.9	0.8	0.000008	14.8	529
2				4.5	64.7	0.07	423 + 4	2.3	1.1	0.000002	13.1	595
3	0.39	456.8 + 6.6	6.0	17.8	71.2	0.25	457 + 4	3.1	0.9	0.000054	15.5	502
4	0.06	445.3 + 6.5	5.9	79.1	1166.3	0.07	445 + 2	1.8	0.8	0.000311	15.9	486
5	0.09	432.1 + 6.5	4.4	17.0	127.5	0.13	433 + 3	2.8	1.0	0.000036	13.8	569
6	0.07	442.3 + 6.4	5.3	36.8	466.8	0.08	442 + 2	1.7	0.9	0.000041	12.4	623
7	0.06	446.5 + 6.5	4.7	6.5	108.4	0.06	447 + 4	1.9	0.7	0.000100	16.5	463
10	0.05	444.9 + 6.5	5.0	4.9	96.7	0.05	445 + 3	1.3	1.1	0.000009	13.8	569
11	0.01	460.6 + 6.7	3.4							0.000407	17.4	428
12	0.19	424.4 + 6.2	4.9	36.5	211.9	0.17	427 + 3	0.7	1.0			
13	0.12	439.7 + 6.4	4.2	16.4	153.1	0.11	440 + 3	2.1	0.8			
14	0.11	427.7 + 6.2	3.8	10.0	144.5	0.07	429 + 4	1.1	1.0			
15	0.15	447.2 + 6.5	5.6	78.8	568.0	0.14	448 + 3	1.0	0.8	0.000033	12.9	602
16	0.09	435.8 + 6.3	3.4							0.000013	14.0	559
17	0.01	422.5 + 6.2	4.6	0.5	49.6	0.01	424 + 5	2.7	1.6	0.000003	12.7	611
18	0.13	457.9 + 6.6	4.0	233.3	1312.6	0.18	457 + 2	0.8	0.9			
19	0.07	453.7 + 6.6	4.1	31.7	408.7	0.08	452 + 2	1.3	1.0	0.000030	14.5	541
20	0.05	429.5 + 6.2	3.9	4.0	60.4	0.07	430 + 4	2.7	1.2	0.000014	16.4	468
21	0.15	443.1 + 6.7	4.3	15.4	121.9	0.13	445 + 3	0.9	0.9	0.000010	15.0	521
22	0.09	436.9 + 6.4	3.6	1.0	31.2	0.03	438 + 6	35.1	0.7	0.000120	13.5	580
23	0.07	447.7 + 6.5	3.8	26.1	276.3	0.09	448 + 3	1.9	0.9			
24	0.07	447.7 + 6.5	5.4	6.7	84.4	0.08	448 + 4	1.3	0.9	0.000014	13.6	576
25	0.01	429.1 + 6.3	5.4	0.6	74.5	0.01	430 + 4	2.6	1.1	0.000004	12.1	636
26	0.05	445.8 + 6.7	3.7	8.4	102.8	0.08	447 + 4	1.6	0.9	0.000076	14.1	555
27	0.09	427.4 + 6.3	3.6	8.3	66.5	0.12	425 + 4	1.1	0.9	0.000004	16.1	478
28				6.0	64.4	0.09	420 + 6	2.9	1.2	0.001045	16.6	456
29				4.1	69.4	0.06	445 + 4	1.9	0.9	0.000038	12.9	602
30				67.9	540.7	0.13	450 + 3	2.1	0.8			
13NQ52 garnet amphibolite												
1	0.04	439.4 + 6.4	5.1	8.7	159.8	0.05	440 + 3	0.5	0.8	0.000002	15.8	489
4c	0.40	457.1 + 6.7	2.9	210.4	304.8	0.69	457 + 2	47.5	0.3	0.001187	14.3	550
6	0.03	433.6 + 6.3	2.9	16.2	570.5	0.03	434 + 2	3.9	0.8	0.000421	13.9	566
7	0.04	435.9 + 6.3	3.0	6.6	163.0	0.04	436 + 3	0.3	1.1	0.000001	12.5	619
8c	0.48	446.1 + 6.5	4.0	41.3	106.4	0.39	458 + 3	71.0	0.5	0.001080	12.7	615
10	0.01	437.5 + 6.4	3.6	3.3	141.6	0.02	438 + 3	46.0	1.0	0.000412	13.7	572
11c	0.50	466.3 + 6.8	4.0	118.4	207.6	0.57	467 + 3	24.3	0.3	0.001918	15.3	511
12	0.02	443.2 + 6.4	3.6	5.5	227.1	0.02	444 + 3	6.2	1.2	0.000196	13.4	583
13	0.10	433.6 + 6.4	3.0							0.000034	12.4	623
14	0.00	433.5 + 6.6	2.8	0.4	83.2	0.01	433 + 5	11.4	0.9	0.000020	14.1	559
15	0.09	447.1 + 6.5	3.2	4.4	51.1	0.09	445 + 4	10.9	1.0	0.000066	13.9	566
16	0.33	446.7 + 6.5	3.9	29.4	94.8	0.31	445 + 5	4.3	0.8	0.000102	15.7	495
17	0.19	443.6 + 6.4	3.5	42.5	210.4	0.20	446 + 3	0.5	0.7	0.000660	13.8	571
18c	0.49	470.6 + 6.9	3.2	76.4	135.7	0.56	471 + 4	39.8	0.5	0.001768	11.8	652
20	0.03	430.5 + 6.3	3.4							0.000022	14.2	553
21	0.05	427.4 + 6.2	3.9	11.9	52.4	0.23	428 + 7	57.5	0.5	0.000063	12.3	626
22c				58.8	139.3	0.42	472 + 3	50.2	0.3			
23c	0.31	474.9 + 6.9	4.8	171.0	403.0	0.42	470 + 2	62.7	0.5	0.001686	15.7	493
24	0.06	444.1 + 6.4	3.5	16.0	254.5	0.06	445 + 3	0.5	0.8	0.000003	13.0	599
25	0.28	432.9 + 6.3	3.7							0.000219	14.3	548
26	0.10	445.5 + 6.5	3.5	16.7	171.0	0.10	447 + 3	0.7	0.9	0.000003	15.0	523
27	0.01	447.8 + 6.5	3.4	4.0	223.2	0.02	449 + 2	38.0	0.8			

Notes:1. Relict magmatic cores are denoted with suffix "c".2. Initial ε_{Hf} values are calculated at t = 830 Ma for samples 09QL86, 09QL93, 09QL105 and 13NQ44; at t = 516 Ma for samples 09QL32, 13NQ02, 13NQ38 and 113NQ52.

415 Ma. In contrast, the CL-bright domains have lowered $\varepsilon_{Hf}(t)$ values of 13.9–19.1 but elevated T_{DM1} ages of 361–564 Ma (Fig. 7d).

4.7. Eclogite 13NQ38 at Yematan

Most zircon grains are CL-bright without zoning, and a few grains have core–rim structure with CL-dark core and CL-bright rim (Fig. 2g). Garnet, omphacite, rutile and quartz inclusions were observed in the measured domains. SIMS dating on most grains yield consistent $^{206}Pb/^{238}U$ ages with a weighted mean of 438 ± 4 Ma, but 4 of the CL-dark cores yield older ages (Fig. 4g). All the zircon domains have Th/U < 0.1, flat HREE patterns without Eu anomalies (Figs. 5d and 6g), similar $\delta^{18}O$ values of 3.4–6.0‰ (Fig. 7c), and roughly similar ε_{Hf}(t = 516 Ma) values of 12.1 to 17.4 and T_{DM1} ages of 428 to 636 Ma (Fig. 7d).

4.8. Garnet amphibolite 13NQ52 at Yematan

Most zircon grains are CL-bright without zoning, and few CL-dark domains with oscillatory zoning occur as cores or grains (Fig. 2h). The CL-dark domains have high contents of Th and U (hundreds of ppm) and high ratios of Th/U (>0.3), yielding $^{206}Pb/^{238}U$ ages of 446 to 475 Ma (Fig. 4h). In contrast, the CL-bright grains have low Th contents (several ppm), low Th/U ratios (generally <0.1) and coherent $^{206}Pb/^{238}U$ ages with a weighted mean of 442 ± 4 Ma (Fig. 4h). The

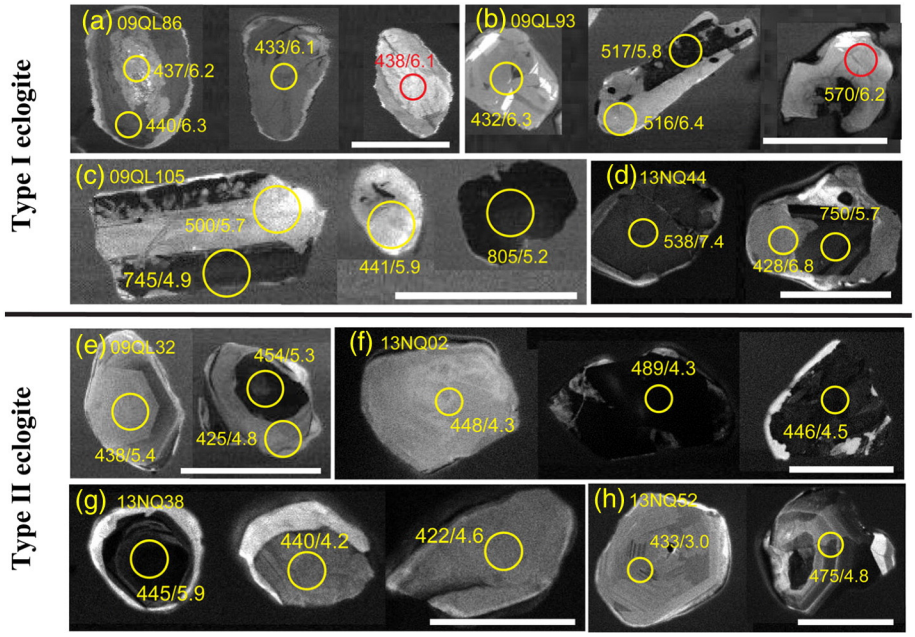

Fig. 2. Representative zircon CL images for eclogites from the North Qaidam orogen. SIMS analytical spot along with $^{206}Pb/^{238}U$ age (left) and $\delta^{18}O$ value (right) are marked in the figure. The scale bar is 100 μm.

cores exhibit steep HREE patterns with significant negative Eu anomalies, whereas the CL-bright domains show lower REE contents with flat to steep HREE patterns and no negative Eu anomalies (Fig. 6h). Nevertheless, both the two zircon domains have similar $\delta^{18}O$ values of 2.8 to 5.1‰ (Fig. 7c), consistent ε_{Hf} (t = 516 Ma) values of 11.8–15.8 and T_{DM1} ages of 489 to 652 Ma (Fig. 7d).

5. Discussion

5.1. Uniform eclogite-facies metamorphic ages across the orogen

Zircon can form over a protracted history from prograde, peak to retrograde metamorphism in deeply subducted continental crust, which is dictated by lithochemistry, P–T conditions and fluid availability (e.g., Hermann et al., 2013; Rubatto and Hermann, 2007; Wu et al., 2006b; Xia et al., 2013; Zheng, 2009). The formation of metamorphic zircon can proceed either by reworking of pre-existing protolith zircon or by newly growing from sub-solidus reaction, aqueous fluids or anatectic melts (e.g., Chen et al., 2010, 2011; Xia et al., 2009). The key in dating metamorphism by zircon is to recognize zircon domains that were fully equilibrated under given metamorphic conditions and to link the episodes of zircon growth to specific metamorphic stages by a combined study of morphology, mineral inclusions, trace elements and isotopes (Chen et al., 2010, 2011; Hermann and Rubatto, 2003; Hermann et al., 2001; Liu and Liou, 2011; Rubatto, 2002; Xia et al., 2009).

The CL-bright zircon domains from sample 09QL86 at Xitieshan, sample 13NQ02 at Shaliuhe, samples 13NQ44, 13NQ38 and 13NQ52 at Yematan exhibit relatively flat HREE patterns and no Eu anomalies (Fig. 6a, d, f, g, h). Compared to the older CL-dark cores, the CL-bright domains show coherent younger ages, generally lower Th, U, Ti, Nb, Ta, P and HREE contents, lower Th/U (generally <0.1) and $(Yb/Gd)_N$ ratios, but higher Hf contents (Fig. 5). These features are typical of metamorphic zircon grown under eclogite-facies conditions (e.g., Bingen et al., 2004; Rubatto, 2002; Whitehouse and Platt, 2003). Mineral inclusions of garnet, omphacite and rutile occur in these domains (Fig. 3), also indicating their growth under eclogite-facies metamorphic conditions. Most of the CL-bright zircon domains of these samples yield similar U–Pb ages of 435–440 Ma within errors (Fig. 8), which document similar eclogite-facies metamorphic ages across the North Qaidam orogen.

Zircon domains in sample 09QL32 at Shaliuhe exhibit no Eu anomalies in REE patterns (Fig. 6e), and contain mineral inclusions of garnet, omphacite and rutile (Fig. 3e, f). They have consistent U–Pb ages with a weighted mean of 438 ± 3 Ma (Fig. 4e), similar to the eclogite-facies metamorphic ages determined by above samples, especially nearby 13NQ02. All these observations suggest that these zircon domains would also grow during eclogite-facies metamorphism. Zircons grown under eclogite-facies metamorphic conditions generally exhibit flat REE patterns due to the coexistence of garnet. However, zircon in sample 09QL32 is different from eclogite-facies metamorphic zircon by their steep HREE patterns. This is commonly attributed to zircon growth either prior to significant garnet growth or in disequilibrium with garnet in a closed system or in an open system. Zircon growth prior to significant garnet growth is not preferred as garnet was found as inclusions in zircon and the age of 09QL32 is not older than that of the zircon with flat HREE patterns in nearby sample 13NQ02. In addition, zircon in sample 09QL32 is also unique in containing higher contents of Th, Nb and Ta but lower contents of Hf (Fig. 5d, e, f). All these features are also quite different from zircon grown in a closed system where element concentrations are buffered by coexisting minerals. Therefore, zircon in sample 09QL32 may grow in an open system where the element supply is unlimited due to fluid influx (Rubatto, 2002).

A few CL-bright zircon domains from samples 09QL93 and 09QL105 have similar trace element compositions to eclogite-facies metamorphic zircon from the other samples (Fig. 5a, b, c). Thus, they also grew during eclogite-facies metamorphism, which is verified by the eclogite-facies mineral inclusions (Fig. 3d). A few domains in sample 09QL93 yield coherent SIMS $^{206}Pb/^{238}U$ ages with a weighted mean of 433 ± 5 Ma (Table 1), consistent with the eclogite-facies metamorphic ages in the other samples. In contrast, the other CL-bright domains have trace element compositions and discordant U–Pb ages similar to the CL-dark cores, with high Th and U contents, high Th/U ratios, and steep HREE patterns with significantly negative Eu anomalies (Figs. 5 and 6). These features suggest that they are relict magmatic zircon with different extents of reworking by metamorphic recrystallization. As shown in the CL images (Fig. 2b, c), the cores are irregularly replaced by penetrating or isolated CL-bright domains to form a mosaic structure. Both the

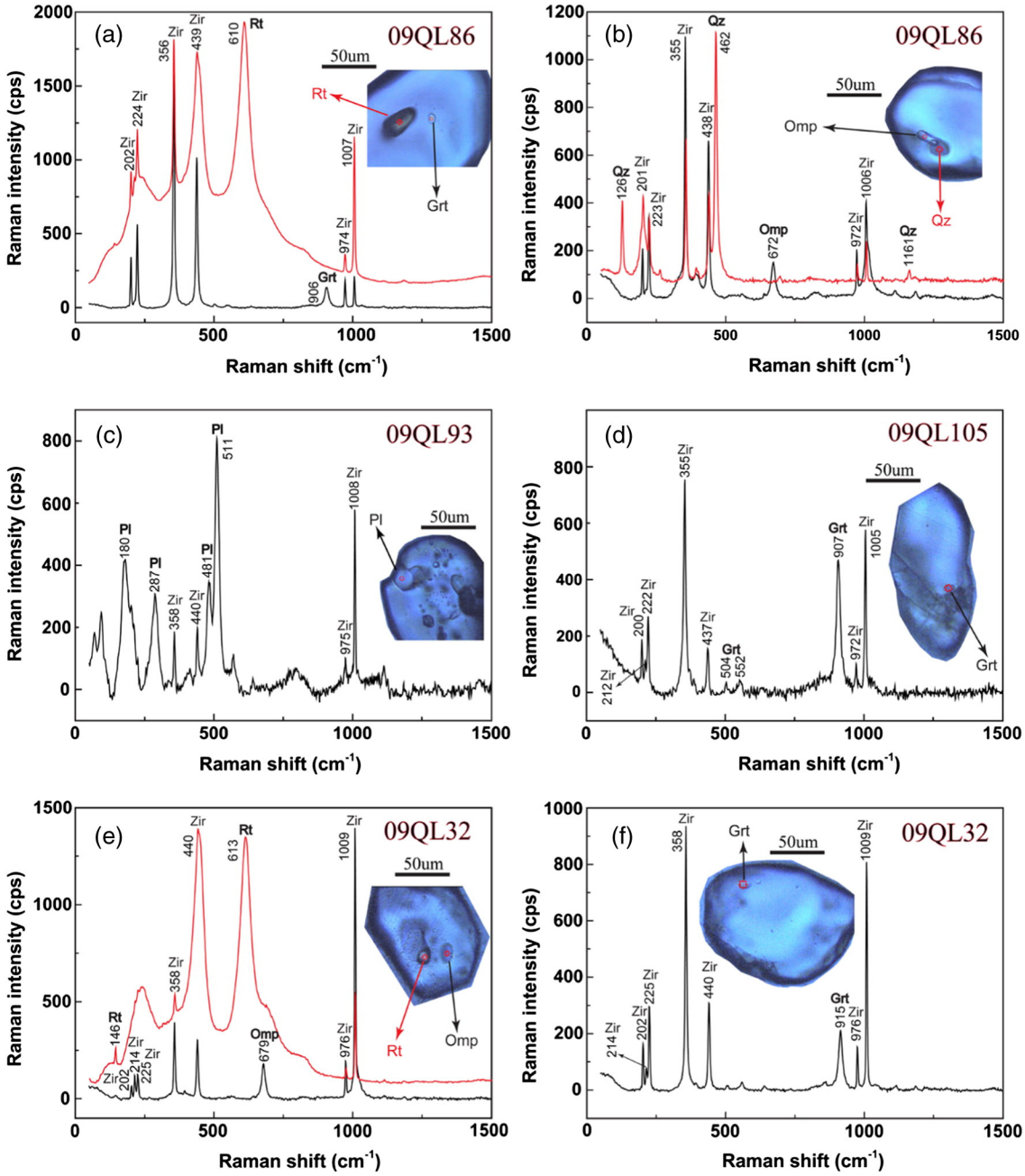

Fig. 3. Representative photographs and Raman spectra of mineral inclusions in zircon from eclogites in the North Qaidam orogen.

internal structure and geochemical features suggest that these CL-bright domains would be formed by dissolution-recrystallization of the cores (Chen et al., 2010, 2011; Rubatto et al., 2008; Spandler et al., 2004; Tomaschek et al., 2003; Xia et al., 2009).

Consistent eclogite-facies metamorphic ages of 433–440 Ma are obtained for eclogites collected across the North Qaidam orogen by the same analytical method (SIMS) in this study (Fig. 8). These ages are also in accord with statistical peak ages obtained for continental-type eclogites from the Yuka, Xiteishan and south Dulan terranes in previous studies (Liu et al., 2012a; Song et al., 2014). On the other hand, a large range in metamorphic ages from 420 to 460 Ma was obtained for eclogites from the Yematan area by previous studies (see review by Song et al., 2014). A few analyses in the present study also yield older or younger ages than 430–440 Ma (Fig. 8). Because the age span of 420 to 460 Ma shows a long period of about 30–40 Myr, there are two different interpretations on them. One school of thoughts interprets the ages to represent prolonged eclogite-facies metamorphism during continental collision (Mattinson et al., 2006; Yu et al., 2013; Zhang et al., 2010). However, some newly grown metamorphic zircons show core–rim structures that record two episodes of eclogite-facies metamorphism at 462–445 Ma and 438–420 Ma, respectively (Song et al., 2014). This leads to another interpretation that links the older and younger ages to two episodes of eclogite-facies metamorphism, respectively, due to the subduction of oceanic crust and continental crust (Song et al., 2014). In this regard, the oceanic-type eclogites in the oceanic subduction zone would have enrolled in the continental subduction zone and experienced a yo-yo subduction like those in the Alps (Rubatto et al., 2011). However, there is no evidence for two cycles of crustal subduction in the North Qaidam orogen. Therefore,

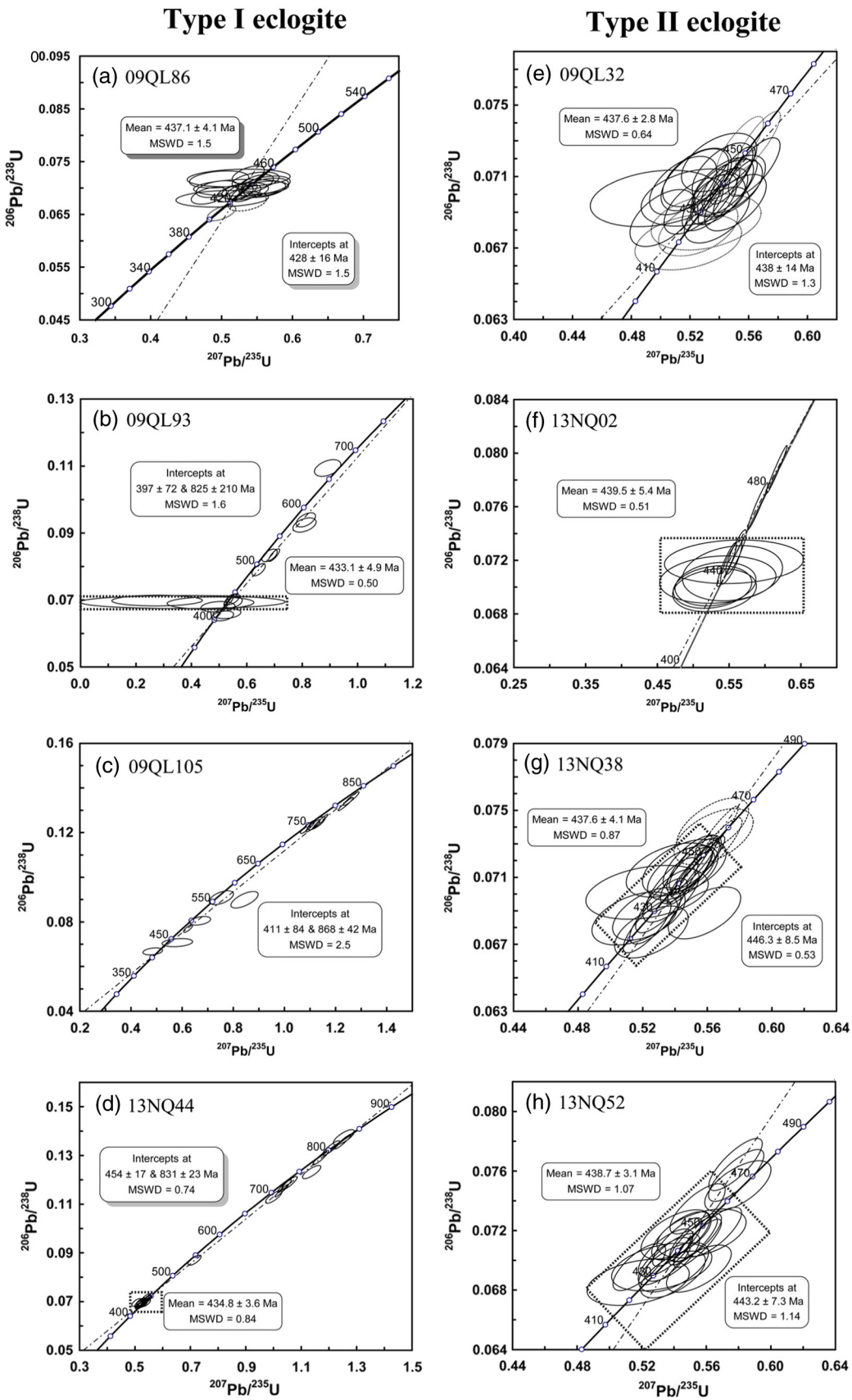

Fig. 4. Concordia diagrams of SIMS zircon U–Pb dating for eclogites from the North Qaidam orogen.

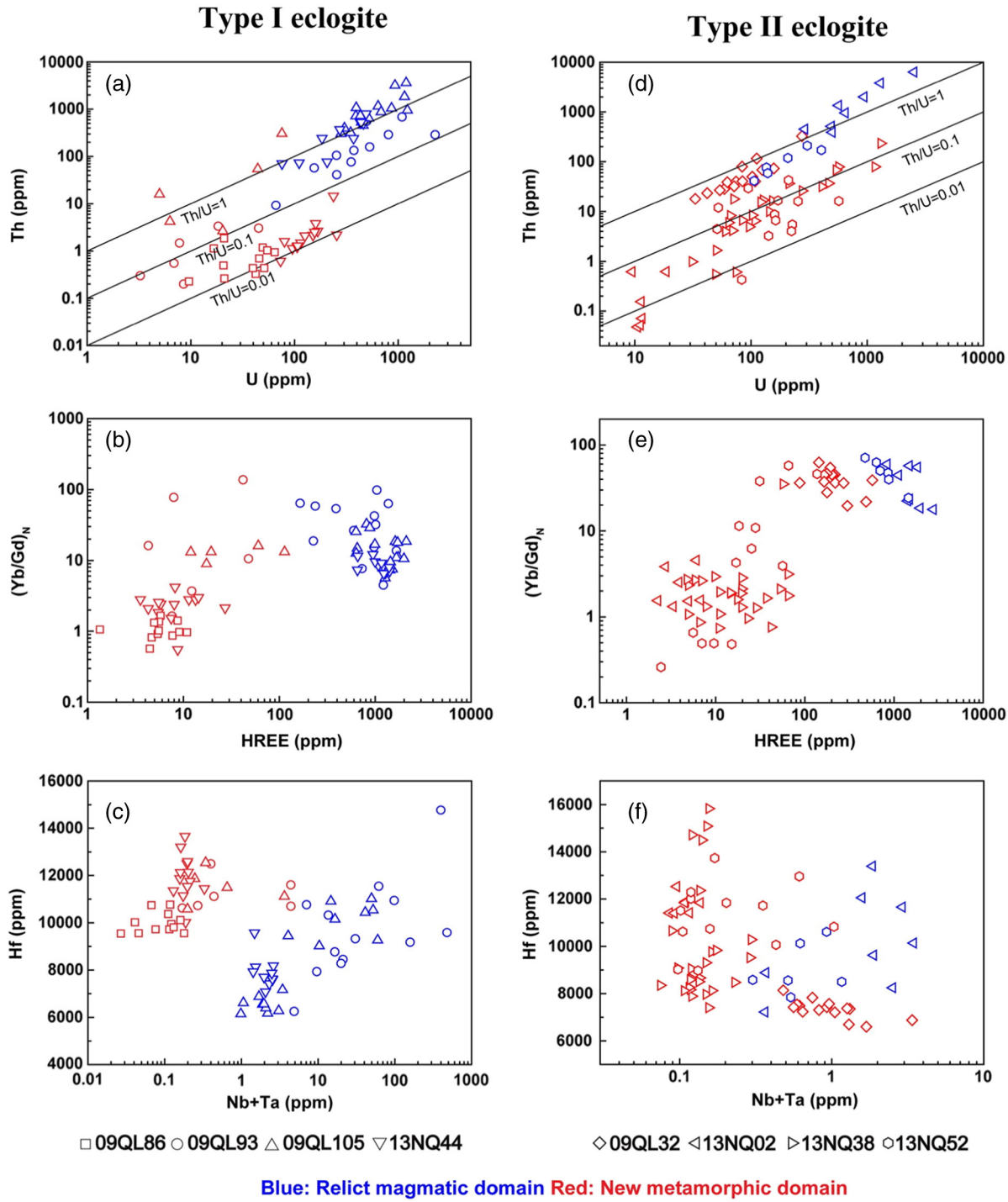

Fig. 5. Correlation diagrams between selected element contents/ratios for zircon from eclogites in the North Qadiam orogen.

the latter interpretation is not preferred unless petrological evidence for multiple HP-UHP events is found within a single sample.

Zircon growth in deeply subducted crust depends on the fluid availability (e.g., Zheng, 2009, 2012). It has been well known that there is only limited fluid action during peak UHP metamorphism, and the main pulse of fluid action for relatively dry eclogites occurs during the initial stage of exhumation due to the exsolution of structural hydroxyl and molecular water from nominally anhydrous minerals (Zheng, 2009, 2012). In this regard, zircon would mainly form during the initial stage of exhumation in the deeply subducted crust (Liu and Liou, 2011; Zheng, 2009). The main age peak of 433–440 Ma in the distribution pattern of zircon U–Pb ages may thus date the eclogite-facies metamorphism in the peak to early exhumation stages. These ages are also similar to the UHP metamorphic ages constrained by coesite-bearing zircon from eclogites in the Xitieshan and south Dulan zones (Liu et al., 2012a; Yu et al., 2013; Zhang et al., 2010). But whether such zircon U–Pb ages from the present study represent the UHP metamorphic ages need further certification by finding of index mineral inclusions. However, minor zircon growth may also occur during prograde and later retrograde metamorphism. Metamorphic zircon with older U–Pb ages (>440 Ma)

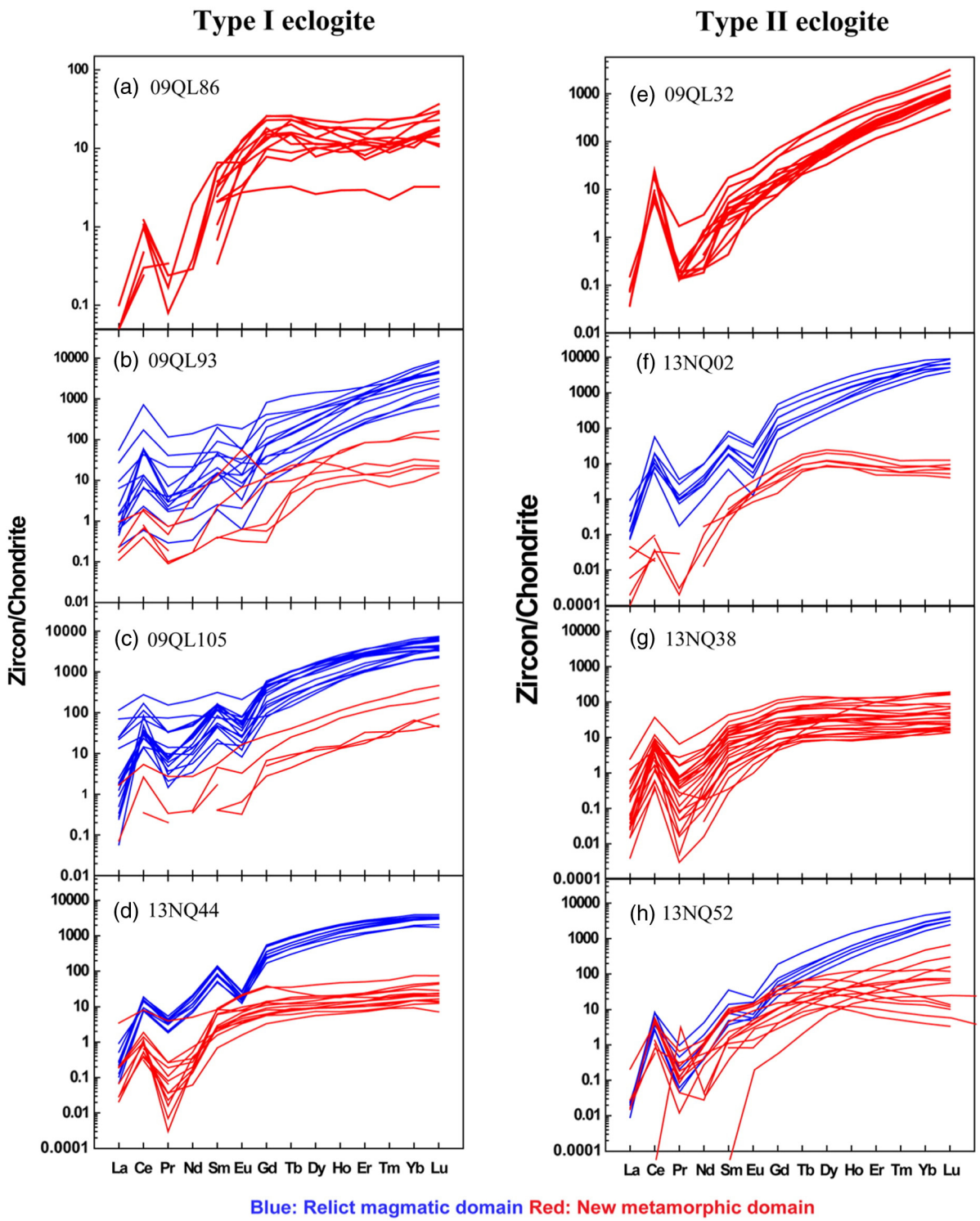

Fig. 6. Chondrite-normalized REE patterns for zircon from eclogites in the North Qaidam orogen. The chondrite values are from Sun and McDonough (1989).

from the Yematan terrane in previous studies mostly have steep HREE patterns (Mattinson et al., 2006; Zhang et al., 2014), suggesting that these zircons may grow during the prograde stage when garnet is in low abundance (Mattinson et al., 2006). Still younger U–Pb ages (<430 Ma), slightly coinciding with granulite-facies overprinting in some terranes (Song et al., 2014), may date the later retrograde stage. Therefore, the features of the older or younger zircons indirectly indicate that the 433–440 Ma age is close to the metamorphic peak age. In summary, it is demonstrated that the eclogites from the North Qaidam orogen may have experienced coeval eclogite-facies metamorphism at 433–440 Ma, regardless of the sample locality and eclogite types.

5.2. Contrasts in the protolith nature of eclogites

The relict magmatic zircon of eclogites provides geochemical fingerprints of the protolith nature while newly grown metamorphic zircon records the metamorphic geochemistry of eclogites. However, protolith zircons could be reworked via different extents of metamorphic recrystallization, leading to partial or complete resetting of U–Pb ages, trace

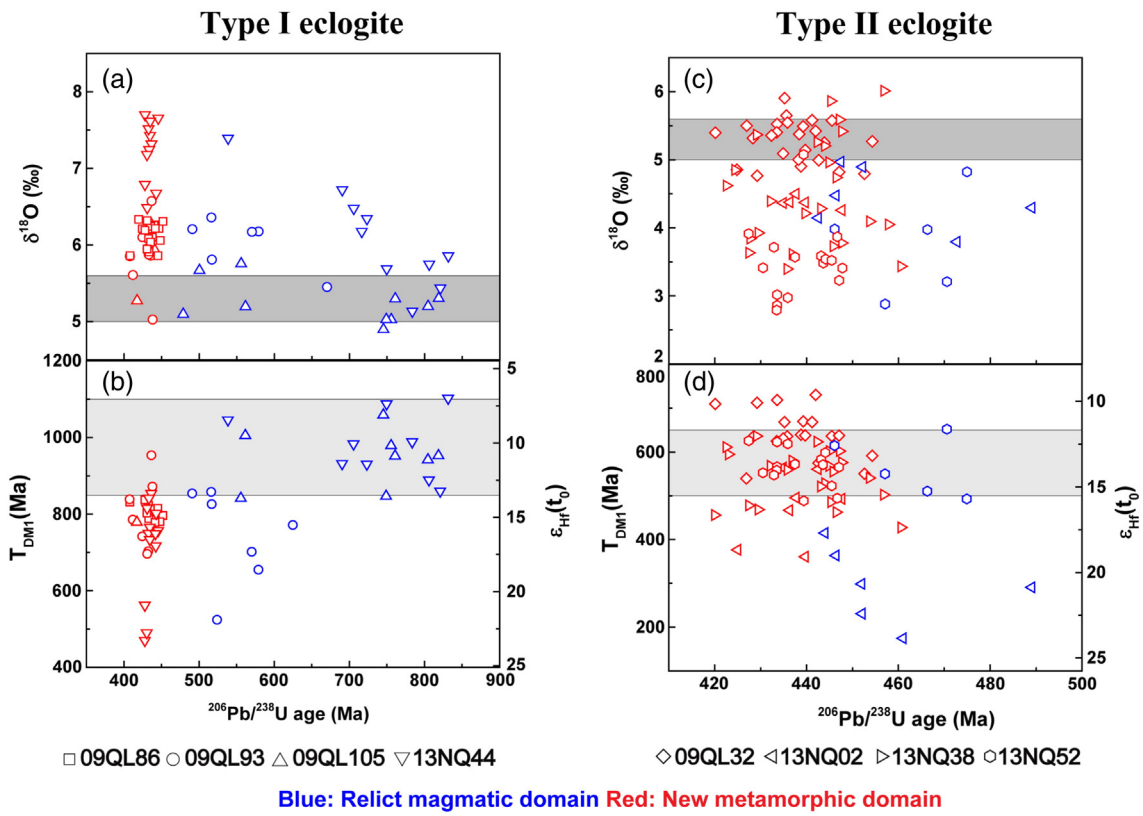

Fig. 7. Zircon O–Hf isotope compositions for eclogites from the North Qaidam orogen. The dark grey bars in (a) and (c) denote the $\delta^{18}O$ ranges of zircon with normal mantle values adopted from Valley et al. (1998). Light grey bars in (b) and (d) denote the protolith Hf compositions. The right axis is related to the left axis by assuming no radiogenic Hf in zircon.

elements and O–Hf isotopes (Chen et al., 2010, 2011; Geisler et al., 2003, 2007; Hoskin and Black, 2000; Liu et al., 2008b, 2012b; Martin et al., 2008; Xia et al., 2009; Zheng et al., 2005, 2006). Therefore, it is essential to discern what are retained during metamorphism. On the other hand, mafic rocks would generally undergo prolonged evolution and sporadic alteration during their stay in the crust and enrollment in subduction zones, and thus generally result in the O–Hf isotopes in metamorphic zircons to deviate from those in the protolith zircons (e.g., Chen et al., 2011; Zheng et al., 2005, 2006). However, if the metamorphic effect can be recognized and removed, the protolith information would also be extractable from metamorphic zircons. In other words, both protolith and metamorphic zircons can shed light on recovering the protolith nature of eclogites.

The relict zircon domains in samples 09QL93 at Xitieshan, sample 09QL105 at Yuka, and sample 13NQ44 at Yematan are characterized by high contents of Th and U, high Th/U ratios (mostly >1), steep HREE patterns with significantly positive Ce and negative Eu anomalies (Figs. 5a and 6b, c, d). These features are typical of magmatic zircon (Chen et al., 2010; Hoskin and Schaltegger, 2003). Blurred oscillatory zoning and variable and discordant U–Pb ages are observed in these cores, suggesting that they have been reworked by metamorphism to different extents. Although their U–Pb dating yield upper incept ages of 825 ± 210 to 866 ± 42 Ma with large uncertainties, some of them have nearly concordant U–Pb ages of 820–830 Ma (Fig. 4b, c, d and Table 1). This suggests that the protolith of these eclogites would have formed in the Middle Neoproterozoic. Relict zircon domains in sample 09QL93 exhibit significantly younger apparent $^{206}Pb/^{238}U$ ages than those in samples 09QL105 and 13NQ44, suggesting that they have undergone more severe metamorphic reworking during the continental collision in the Early Paleozoic.

The CL-dark cores in samples 13NQ02 at Shaliuhe and 13NQ52 at Yematan also exhibit geochemical features typical of magmatic zircon

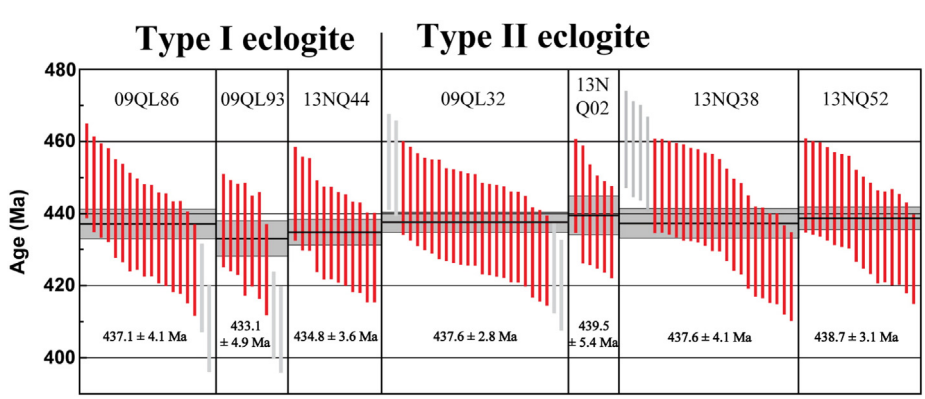

Fig. 8. A summary diagram of metamorphic ages for zircon from eclogites in the North Qaidam orogen. All data are shown in 2σ errors. Thick horizontal lines represent the weighted mean ages given in the bottom. Light grey bars are not included in calculating the weighted means.

that are similar to relict cores in samples 09QL93, 09QL105 and 13NQ44 (Fig. 5f, h) and different from eclogite-facies metamorphic zircon domains (Figs. 5 and 6), but have variable U–Pb ages with the SIMS $^{206}Pb/^{238}U$ ages of 440–489 Ma and 446–475 Ma, respectively (Fig. 4f, h). In the case of scattering ages for the relict cores, the oldest concordant age of 489 ± 7 Ma is taken as the minimum age of eclogite protolith. Previous dating of zircon from a kyanite eclogite at Shaliuhe suggests that it has protolith U–Pb age of 516 ± 8 Ma (Zhang et al., 2008). Therefore, the protolith of these eclogites would have formed in the Cambrian. In this regard, there are two types of eclogites with different protolith ages of >830 Ma in the Neoproterozoic and >489 Ma in the Cambrian, respectively.

The two types of eclogites are more easily distinguished by their zircon O isotope compositions (Fig. 7a). Most zircon grains from samples 09QL86, 09QL93, 09QL105 and 13NQ44 (Type I eclogites) have ^{18}O values similar to or higher than normal mantle values of 5.3 ± 0.3‰ (Valley et al., 1998). Previous studies have demonstrated that metamorphic recrystallization would reset the O isotope composition of protolith zircon, and relict magmatic zircon that retained protolith U–Pb ages can preserve the primary O isotope composition (Chen et al., 2011). There is a roughly negative correlation between $\delta^{18}O$ values and $^{206}Pb/^{238}U$ ages for zircons in Type I eclogites (Fig. 7a), indicating the presence of metamorphic effect. Nevertheless, it also reveals that the relict zircon with U–Pb ages close to the protolith age have mantle-like $\delta^{18}O$ values (Fig. 7a). These observations suggest that the protolith of Type I eclogite should be mafic igneous rocks with mantle-like $\delta^{18}O$ values and their $\delta^{18}O$ values are elevated during their stay in the crust or enrollment in the subduction zone. In this regard, the high $\delta^{18}O$ values could not be caused by fractional crystallization or crustal contamination during magma ascent. This is also confirmed by the following two observations: (1) fractional crystallization could lead to a large increase in $\delta^{18}O$ values only when MgO content is reduced to less than 2% (Eiler, 2001), which is not evident in Type I eclogites; (2) crustal contamination is minor as Type I eclogites are mostly depleted in melt-mobile incompatible trace elements and radiogenic Sr–Nd isotopes. The high $\delta^{18}O$ values of metamorphic zircon in these samples indicate that the fluid from which metamorphic zircon grew has high $\delta^{18}O$ values. This further suggests that these eclogites acquired high $\delta^{18}O$ values by either low temperature alteration of their protolith or metasomatism by high $\delta^{18}O$ fluids released from surrounding gneisses during subduction-zone metamorphism (Liu et al., 2014). Metamorphic zircon could acquire high $\delta^{18}O$ values if they are formed in the presence of fluids released from high $\delta^{18}O$ gneisses. Although this possibility cannot be completely excluded at present, previous studies have demonstrated that fluids are generally internally buffered during eclogite-facies metamorphism in continental subduction zones (Zheng, 2009; Zheng et al., 2003). Therefore, the high $\delta^{18}O$ values for Type I eclogites were most likely acquired by the low temperature water–rock interaction of mafic protolith.

In contrast, zircon grains from samples 09QL32, 13NQ02, 13NQ38 and 13NQ52 (Type II eclogites) generally have $\delta^{18}O$ values similar to or lower than the normal mantle values (Fig. 7c). This suggests that the protolith of Type II eclogites should have directly or indirectly experienced high-temperature fluid–rock interaction to result in the lowered $\delta^{18}O$ values. However, the low $\delta^{18}O$ values can hardly originate from low ^{18}O magmas though a few relict magmatic cores have low $\delta^{18}O$ values (Fig. 7c). This is because mafic igneous rocks with low $\delta^{18}O$ values can only be derived from partial melting of mantle sources that have been metasomatized by low $\delta^{18}O$ crustal fluids/melts (Zheng et al., 2004). This is typified by low $\delta^{18}O$ values for postcollisional mafic rocks from the Dabie orogen in east-central China (Dai et al., 2011). The low $\delta^{18}O$ mafic rocks exhibit arc-like trace element distribution patterns due to crustal metasomatism (Dai et al., 2011), which are absent in Type II eclogites. Therefore, the low $\delta^{18}O$ values of relict zircon cores are not primary but instead are reworked by low $\delta^{18}O$ fluids during the eclogite-facies metamorphism. Therefore, the low $\delta^{18}O$ values of Type II eclogites were acquired by high temperature hydrothermal alteration during magma intrusion.

These two types of eclogites also differ in Hf isotopes. Zircon from Type I ecclogites generally has T_{DM1} age >700 Ma (Fig. 7b), whereas zircon from Type II eclogites generally has T_{DM1} age < 700 Ma (Fig. 7d). Previous studies have demonstrated that the protolith zircon domains generally preserve unchanged Hf isotopes despite different extents of recrystallization. For a newly grown zircon from metamorphic fluids or anatectic melts, its Hf isotopes would be same as the protolith zircon if the Hf source is mainly derived from the protolith zircons, otherwise its Hf isotopes would become more radiogenic if high Lu/Hf minerals dominate the Hf source of the newly grown zircon (Chen et al., 2010, 2011; Liu et al., 2008b; Xia et al., 2009; Zheng et al., 2005). The relict protolith zircon cores that have U–Pb ages close to the upper intercept ages from Type I eclogites have positive $\varepsilon_{Hf}(t = 830\ Ma)$ values of 7.3–13.8 and T_{DM1} ages of 850–1100 Ma (Fig. 7b), which can be taken as the Hf isotope values for the eclogite protolith. In contrast, the newly grown zircons and severely reworked relict cores have elevated ε_{Hf} values and decreased T_{DM1} ages (Fig. 7b), indicating incorporation of the external Hf into these zircon domains.

Zircon from Type II eclogites mostly has positive $\varepsilon_{Hf}(t)$ values and T_{DM1} ages of 500–650 Ma (Fig. 7d). The metamorphic domains mostly have similar Hf isotope values to the relict cores (e.g., from 13NQ52), indicating the Hf isotope inheritance from the protolith zircon to the metamorphic zircon. Some zircon grains from sample 09QL32 have older Hf model ages, suggests incorporation of isotopically enriched components into the protolith source of sample 09QL32. The protolith zircon cores in sample 13NQ02 have extremely high $\varepsilon_{Hf}(t)$ values and young T_{DM1} ages that are even younger than metamorphic domains and ages. This is quite unusual as metamorphic effect usually leads to elevated $\varepsilon_{Hf(t)}$ values and reduced T_{DM1} ages for metamorphic zircon, compared with protolith zircon. One possible explanation is that the protolith zircon would be crystallized from the part of magma chamber with extremely radiogenic Hf in disequilibrium with the rest part of the magma chamber. Nevertheless, more evidence is needed to clarify this issue in the future.

In summary, the two types of eclogites in the North Qaidam orogeny show a series of differences in their zircon U–Pb ages and Hf–O isotopes. The first type of eclogites has the Neoproterozoic protolith U–Pb ages of >830 Ma, the zircon T_{DM1} ages of about 850–1100 Ma, and the mantle-like $\delta^{18}O$ values for the relict magmatic zircon but elevated $\delta^{18}O$ values for the metamorphic zircon. The high $\delta^{18}O$ values of eclogites are the result of low temperature alteration during residence of their magmatic protolith in the crust. The single-stage Hf model ages are close to the protolith U–Pb age, with the youngest ones nearly same as the protolith U–Pb age. This suggests that these eclogites record growth and reworking of the juvenile crust in the early Neoproterozoic. The second type of eclogites has the Cambrian protolith U–Pb ages of >489 Ma, the zircon T_{DM1} ages of about 500–650 Ma and the mostly low zircon $\delta^{18}O$ values. The low $\delta^{18}O$ values of eclogites are due to high temperature hydrothermal alteration during intrusion of their magmatic protolith. The T_{DM1} ages are only slightly older that the Cambrian protolith U–Pb ages, suggesting that the mafic protolith of these eclogites were extracted from extremely depleted mantle in the early Paleozoic.

Type I eclogites have a large time interval between the protolith and metamorphic ages (approaching 400 Myr), which is much longer than the maximum age of oceanic crust (about 200 Ma). Thus, they are suggested to be metamorphosed from Neoproterozoic continental mafic igneous rocks. The high $\delta^{18}O$ values for some Type I eclogites are consistent with low temperature alteration of the continental basalts at shallow depth. The Qaidam Block has a similar tectonic evolution to the Tarim and South China Blocks during the Grenvillian orogenesis, and all the three blocks are considered parts of the Rodinia supercontinent (Song et al., 2012; Zheng et al., 2013b). Neoproterozoic continental basalts also occur in the Tarim and South China Blocks, and they have a petrogenetic link to the breakup of Rodinia (Li et al., 2009; Zhang and

Zheng, 2013; Zhang et al., 2011). In the North Qinling and Dabie–Sulu orogens, the Neoproterozoic basalts were subducted to mantle depths in the early Paleozoic and early Mesozoic, respectively, transforming them into UHP eclogites (Wu and Zheng, 2013; Zheng et al., 2013b). Neoproterozoic basalts with similar ages to the protolith of Type I eclogites have also been found in the North Qaidam orogen (Zhu et al., 2015). Therefore, Type I eclogites are also suggested to be metamorphosed from continental rift basalts in response to the breakup of Rodinia (Song et al., 2010). Previous studies have also revealed that eclogites, with Neoproterozoic protolith ages (>750 Ma) and early Paleozoic metamorphic ages (460–420 Ma), mostly have geochemical features similar to continental rift/flood basalts (Chen et al., 2009; Song et al., 2010; Yu et al., 2013; Zhang et al., 2013b).

The igneous precursors of Type II eclogites were extracted from the depleted mantle in the Cambrian and experienced high temperature water–rock interaction during magma emplacement. During this period, there are the generation and subduction of oceanic crust prior to the continental subduction in the North Qaidam orogen (e.g., Shi et al., 2006; Song et al., 2014; Zhu et al., 2015). Therefore, the protolith of Type II eclogites may be mafic oceanic crust that is depleted in radiogenic Nd and Hf isotopes and susceptible to seawater hydrothermal alteration. Relict magmatic zircon in some Type II eclogites suggest the eclogites were metamorphosed from oceanic gabbros, as oceanic basalts cannot be saturated in Zr for zircon growth (Grimes et al., 2007, 2009). This is in accordance with the fact that oceanic gabbros acquire their low $\delta^{18}O$ values by high temperature hydrothermal alteration (Gregory and Taylor, 1981; Muehlenbachs, 1986), and subducted crusts could preserve the anomalous $\delta^{18}O$ value (Barnicoat and Cartwright, 1995; Zheng et al., 2003, 2004). Previous geochemical studies for eclogites from two cross sections in the Yematan and Shaliuhe areas of the Dulan terrane also found the similarity between the eclogites and oceanic mafic igneous rocks, with a kyanite eclogite at Shaliuhe yielding a protolith U–Pb age of 516 ± 8 Ma (Song et al., 2003; Zhang et al., 2008). All these observations argue for the origination of Type II eclogites from the oceanic crust. The geochemical compositions of these eclogites may cause some confusion (Yu et al., 2013; Zhang et al., 2010), but the quite different zirconology from Type I eclogites definitely indicate a different origin for the protolith of Type II eclogites. However, the eclogites from Shaliuhe and Yemantan are not all metamorphosed from the subducted oceanic crust as exemplified by sample 13NQ44. In this regard, both continental- and oceanic-type eclogites occur in the Dulan terrane, whereas only continental-type eclogites occur in the Xitieshan and Yuka terranes.

6. Implications for the tectonic transition from oceanic subduction to continental subduction

The coexistence of oceanic- and continental-type eclogites in the North Qaidam orogen records the tectonic transition from oceanic subduction to continental subduction in the early Paleozoic. In general, there is a time lag between the subduction of oceanic crust and the collision of continental blocks, e.g., about 10 Myr in the western Alps (Rubatto et al., 1998) and about 80 Myr in the Hong'an orogen (Wu and Zheng, 2013; Zhou et al., 2015). However, the eclogite-facies metamorphic ages constrained by oceanic-type eclogites (Type II) and by continental-type eclogites (Type I) are nearly the same in the North Qaidam orogen, though the former may be statistically a little older in average (Fig. 8). This suggests that the time discrepancy between the subduction of oceanic crust and continental crust is quite short, nearly within analytical errors. There are two possibilities to explain the dating results. The first is rapid consumption of the oceanic basin as soon as subduction began, which was immediately followed by subduction of continental crust. Thus, the oceanic basin may be a small marginal basin such as a backarc basin because a marginal basin is short-lived and would be consumed rapidly within a few million years (Hall, 2002). In contrast, a mature oceanic basin has a long subduction history. In addition, the subducted oceanic crust was brought up along with the continental crust without decoupling at mantle depths. The second is that the oceanic-type eclogites represent the oceanic crust that resides at the continent–ocean transition. Small amounts of oceanic-type eclogites were entrained by exhuming continental crust after the breakoff of subducted oceanic slab from the continental slab. Therefore, the exhumed oceanic-type eclogites share the similar metamorphic evolution to the continental-type eclogites. As oceanic subduction initiated much earlier than the presently determined metamorphic ages (Shi et al., 2006; Song et al., 2014; Zhu et al., 2015), the second possibility is preferred. On the other hand, it is generally thought that deeply subducted oceanic slab is hardly to exhume due to its high density. The exhumed oceanic-type eclogites in the present study implies that exhumation of high-density oceanic-type eclogites is entrained by associated low-density continental crust along the same subduction channel (Guillot et al., 2009; Zheng et al., 2013a).

Major stages in the tectonic evolution from oceanic subduction to continental subduction revealed by this study is illustrated by a schematic sketch (Fig. 9), and summarized as follows. (a) Continental basalts are generated in the Middle Neoproterozoic in response to the breakup of Rodinia. The opening of an oceanic basin before the continental subduction separates the Qaidam Block from the Qilian block at >460 Ma ago. The Qaidam Block, on the side of passive continental margin, is dragged towards the Qilian Block by the subducting oceanic slab. (b) Consumption of the oceanic crust finally led to the collision between the Qaidam and Qilian Blocks. Subduction of the continental crust was driven by the oceanic slab with eclogite-facies metamorphism of its overlying crust, and the continental crust experienced HP to UHP eclogite-facies metamorphism at 460–420 Ma. (c) At about 430 Ma, deeply subducted continental crust was detached from the dense oceanic slab and started exhumation. At the transition zone between continental and oceanic slabs, the attached small slices of oceanic crust (including oceanic-type eclogites) were entrained into the exhuming continental crust. These oceanic-type eclogites formed in the transitional zone thus share the similar metamorphic evolution with the continental-type eclogites. (d) Oceanic-type eclogites were brought up together with the continental-type eclogites and thus dismembered in the latter unit.

7. Conclusions

Zircon U–Pb dating and O–Hf isotope analyses allow discrimination oceanic-type eclogites from continental-type eclogites in the North Qaidam orogen. The continental-type eclogites have Neoproterozoic protolith ages of >830 Ma and Hf model ages of 850–1100 Ma. The O isotope analysis of relict magmatic zircon and metamorphic zircon reveals that the protolith basalts originally would have mantle-like $\delta^{18}O$ values, but were variably elevated due to low temperature alteration during magma emplacement. Thus this type of eclogites was metamorphosed from Neoproterzoic continental basalts generated during the breakup of supercontinent Rodinia. In contrast, the oceanic-type eclogites have Cambrian protolith ages of >489 Ma and Hf model ages of 500–650 Ma. The low $\delta^{18}O$ values of zircon suggest that the eclogite protoliths underwent high temperature seawater-hydrothermal alteration. Thus this type of eclogites was derived from metamorphism of subducted oceanic crust rocks that preceded the subduction of continental crust. These two different types of eclogites record the tectonic transition from oceanic subduction to continental subduction in the early Paleozoic. However, all eclogites across the North Qaidam orogen show consistent eclogite-facies metamorphic ages at 430–440 Ma, regardless of eclogite localities and types. As such, the oceanic-type eclogites share a similar metamorphic evolution with the continental-type eclogites, and therefore they were originated from oceanic segments closely linked to the subducted continental crust and were exhumed along with the subducted continental crust in the continental subduction channel.

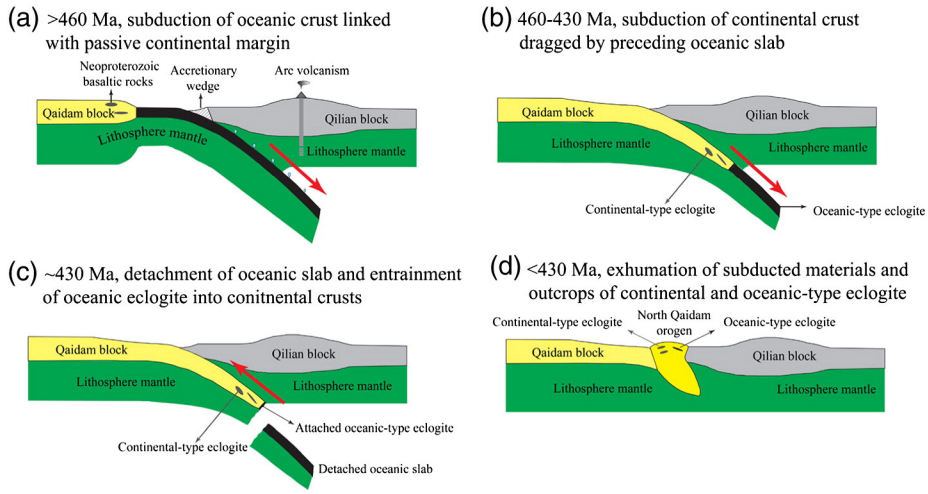

Fig. 9. A schematic sketch showing the tectonic evolution of the North Qaidam orogen. See detailed explanations in the text.

Supplementary data to this article can be found online at http://dx.doi.org/10.1016/j.lithos.2015.12.003.

Acknowledgments

This study was supported by funds from the Chinese Ministry of Science and technology (2015CB856106), the Natural Science Foundation of China (41422301, 41372073 and 41173013), a Foundation for the Author of National Excellent Doctoral Dissertation of PR China (201229) and Program for New Century Excellent Talents in University (NCET-11-0875). Thanks are due to Hai-Yong Li, Chun-Yang Liu and Meng Yu for their assistance in the field, to Qiuli Li, Yu Liu and Guoqiang Tang for their assistance with the SIMS analyses in Beijing, to Fukun Chen and Yizeng Yang for their assistances with the laser Raman analysis. We appreciate two anonymous reviewers for their comments and Dr. Marco Scambelluri for his editorial handling.

References

Andersen, T., 2002. Correction of common lead in U–Pb analyses that do not report ^{204}Pb. Chemical Geology 192, 59–79.
Barnicoat, A.C., Cartwright, I., 1995. Focused fluid flow during subduction: oxygen isotope data from high-pressure ophiolites of the western Alps. Earth and Planetary Science Letters 132, 53–61.
Beltrando, M., Compagnoni, R., Lombardo, B., 2010. (Ultra-) high-pressure metamorphism and orogenesis: an Alpine perspective. Gondwana Research 18, 147–166.
Bingen, B., Austrheim, H., Whitehouse, M.J., Davis, W.J., 2004. Trace element signature and U–Pb geochronology of eclogite-facies zircon, Bergen Arcs, Caledonides of Western Norway. Contributions to Mineralogy and Petrology 147, 671–683.
Bouvier, A., Vervoort, J.D., Patchett, P.J., 2008. The Lu–Hf and Sm–Nd isotopic composition of CHUR: constraints from unequilibrated chondrites and implications for the bulk composition of terrestrial planets. Earth and Planetary Science Letters 273, 48–57.
Chen, D.-L., Liu, L., Sun, Y., Liou, J.-G., 2009. Geochemistry and zircon U–Pb dating and its implications of the Yukahe HP/UHP terrane, the North Qaidam, NW China. Journal of Asian Earth Sciences 35, 259–272.
Chen, R.X., Zheng, Y.F., Xie, L.W., 2010. Metamorphic growth and recrystallization of zircon: distinction by simultaneous in-situ analyses of trace elements, U–Th–Pb and Lu–Hf isotopes in zircons from eclogite-facies rocks in the Sulu orogen. Lithos 114, 132–154.
Chen, Y.X., Zheng, Y.-F., Chen, R.-X., Zhang, S.-B., Li, Q.L., Dai, M.N., Chen, L., 2011. Metamorphic growth and recrystallization of zircons in extremely 18O-depleted rocks during eclogite-facies metamorphism: evidence from U–Pb ages, trace elements, and O–Hf isotopes. Geochimica et Cosmochimica Acta 75, 4877–4898.
Chopin, C., 1984. Coesite and pure pyrope in high-grade blueschists of the western Alps: a first record and some consequence. Contributions to Mineralogy and Petrology 86, 107–118.
Chopin, C., 2003. Ultrahigh-pressure metamorphism: tracing continental crust into the mantle. Earth and Planetary Science Letters 212, 1–14.
Compagnoni, R., Rolfo, F., 2003. UHPM units in the Western Alps. In: Carswell, D.A., Compagnoni, R. (Eds.), Ultrahigh Pressure Metamorphism. European Mineralogical Union Notes in Mineralogy 5, pp. 13–49.
Dai, L.-Q., Zhao, Z.-F., Zheng, Y.-F., Li, Q., Yang, Y., Dai, M., 2011. Zircon Hf–O isotope evidence for crust–mantle interaction during continental deep subduction. Earth and Planetary Science Letters 308, 224–244.
Davies, J.H., von Blanckenburg, F., 1995. Slab breakoff: a model of lithosphere detachement and its test in the magmatism and deformation of collisional orogens. Earth and Planetary Science Letters 129, 85–102.
Eiler, J.M., 2001. Oxygen isotope variations of basaltic lavas and upper mantle rocks. In: Valley, J.W., Cole, D.R. (Eds.), Stable Isotope Geochemistry. Reviews in Mineralogy and Geochemistry 43, pp. 319–364.
Ernst, W.G., Maruyama, S., Walis, S.R., 1997. Buoyancy-driven, rapid exhumation of ultrahigh-pressure metamorphosed continental crust. Proceedings of the National Academy of Sciences 94, 9532–9537.
Geisler, T., Pidgeon, R.T., Kurtz, R., van Bronswijk, W., Schleicher, H., 2003. Experimental hydrothermal alteration of partially metamict zircon. American Mineralogist 88, 1496–1513.
Geisler, T., Schaltegger, U., Tomaschek, F., 2007. Re-equilibration of zircon in aqueous fluids and melts. Elements 3, 43–50.
Gilotti, J.A., 2013. The realm of ultrahigh-pressure metamorphism. Elements 9, 255–260.
Gregory, R.T., Taylor, H.P., 1981. An oxygen isotope profile in a section of Cretaceous oceanic crust, Samail ophiolite, Oman: evidence for δ^{18}O buffering of the oceans by deep (>5 km) seawater-hydrothermal circulation at mid-ocean ridges. Journal of Geophysical Research 86 (B4), 2737–2755.
Griffin, W.L., Pearson, N.J., Elusive, E., Jackson, S.E., van Achtenberg, E., O'Reilly, S.Y., She, S.R., 2000. The Hf isotope composition of carbonic mantle: LA-MC-ICPMS analysis of zircon megacrysts in kimberlites. Geochimica et Cosmochimica Acta 64, 133–147.
Grimes, C.B., John, B.E., Kelemen, P.B., Mazdab, F., Wooden, J.L., Cheadle, M.J., Hanghøj, K., Schwartz, J.J., 2007. The trace element chemistry of zircons from oceanic crust: a method for distinguishing detrital zircon provenance. Geology 35, 643–646.
Grimes, C.B., John, B.E., Cheadle, M.J., Mazdab, F.K., Wooden, J.L., Swapp, S., Schwartz, J.J., 2009. On the occurrence, trace element geochemistry, and crystallization history of zircon from in situ ocean lithosphere. Contributions to Mineralogy and Petrology 158, 757–783.
Guillot, S., Hattori, K., Agard, P., Schwartz, S., Vidal, O., 2009. Exhumation processes in oceanic and continental subduction contexts: a review. Subduction Zone Geodynamics. Springer, Berlin Heidelberg, pp. 175–205.
Hall, R., 2002. Cenozoic geological and plate tectonic evolution of SE Asia and the SW Pacific: computer-based reconstructions, model and animations. Journal of Asian Earth Sciences 20, 353–431.
Hanchar, J.M., Hoskin, P.W.O., 2003. Zircon. Reviews in Mineralogy and Geochemistry 53, 1–500.
Harley, S.L., Kelly, N.M., 2007. Zircon tiny but timely. Elements 3, 13–18.
Hawkesworth, C.J., Kemp, A.I.S., 2006. Using hafnium and oxygen isotopes in zircons to unravel the record of crustal evolution. Chemical Geology 226, 144–162.
Hermann, J., Rubatto, D., 2003. Relating zircon and monazite domains to garnet growth zones: age and duration of granulite facies metamorphism in the Val Malenco lower crust. Journal of Metamorphic Geology 21, 833–852.
Hermann, J., Rubatto, D., Korsakov, A., Shatsky, V., 2001. Multiple zircon growth during fast exhumation of diamondiferous, deeply subducted continental crust (Kokchetav Massif, Kazakhstan). Contributions to Mineralogy and Petrology 141, 66–82.
Hermann, J., Zheng, Y.-F., Rubatto, D., 2013. Deep fluids in subducted continental crust. Elements 9, 281–288.
Hoskin, P.W.O., Black, L.P., 2000. Metamorphic zircon formation by solid-state recrystallization of protolith igneous zircon. Journal of Metamorphic Geology 18, 423–439.
Hoskin, P.W.O., Schaltegger, U., 2003. The composition of zircon and igneous and metamorphic petrogenesis. Reviews in Mineralogy and Geochemistry 53, 27–55.
Iizuka, T., Hirata, T., 2005. Improvements of precision and accuracy in in situ Hf isotope microanalysis of zircon using the laser ablation-MC-ICPMS technique. Chemical Geology 220, 121–137.

Jackson, S.E., Pearson, N.J., Griffin, W.L., Belousova, E.A., 2004. The application of laserablation-inductively coupled plasma-mass spectrometry to in situ U–Pb zircon geochronology. Chemical Geology 211, 47–69.
Li, Z.X., Li, X.H., Wang, X.C., et al., 2009. 860–750 Ma Large Igneous Provinces in South China: Record of Plume Events During the Breakup of the Supercontinent Rodinia. http://www.largeigneousprovinces.org/09may.
Li, X.-H., Li, W.-X., Li, Q.-L., Wang, X.-C., Liu, Y., Yang, Y.-H., 2010a. Petrogenesis and tectonic significance of the 850 Ma Gangbian alkaline complex in South China: evidence from in situ zircon U–Pb dating, Hf–O isotopes and whole-rock geochemistry. Lithos 114, 1–15.
Li, X.-H., Long, W.-G., Li, Q.-L., Liu, Y., Zheng, Y.-F., Yang, Y.-H., Chamberlain, K.R., Wan, D.-F., Guo, C.-H., Wang, X.-C., Tao, H., 2010b. Penglai zircon megacrysts: a potential new working reference material for microbeam determination of Hf–O isotopes and U–Pb age. Geostandards and Geoanalytical Research 117–134.
Li, X.-H., Tang, G., Guo, B., Yang, Y., Hou, K., Hu, Z., Li, Q., Liu, Y., Li, W., 2013. Qinghu zircon: a working reference for microbeam analysis of U–Pb age and Hf and O isotopes. Chinese Science Bulletin 58, 4647–4654.
Liou, J.G., Ernst, W.G., Song, S.G., Jahn, B.-m., 2009. Tectonics and HP–UHP metamorphism of northern Tibet-preface. Journal of Asian Earth Sciences 35, 191–198.
Liu, F.L., Liou, J.G., 2011. Zircon as the best mineral for P–T–time history of UHP metamorphism: a review on mineral inclusions and U–Pb SHRIMP ages of zircons from the Dabie–Sulu UHP rocks. Journal of Asian Earth Sciences 40, 1–39.
Liu, Y.S., Hu, Z.C., Gao, S., Günther, D., Xu, J., Gao, C., Chen, H., 2008a. In situ analysis of major and trace elements of anhydrous minerals by LA-ICP-MS without applying an internal standard. Chemical Geology 257, 34–43.
Liu, F.L., Gerdes, A., Zeng, L.S., Xue, H.M., 2008b. SHRIMP U–Pb dating, trace elements and the Lu–Hf isotope system of coesite-bearing zircon from amphibolite in the SW Sulu UHP terrane, eastern China. Geochimica et Cosmochimica Acta 72, 2973–3000.
Liu, Y.S., Gao, S., Hu, Z.C., Gao, C., Zong, K., Wang, D., 2010. Continental and oceanic crust recycling-induced melt-peridotite interactions in the Trans-North China Orogen: U–Pb dating, Hf isotopes and trace elements in zircons from mantle xenoliths. Journal of Petrology 51, 537–571.
Liu, X.C., Wu, Y.B., Gao, S., Liu, Q., Wang, H., Qin, Z.W., Li, Q.L., Li, X.H., Gong, H.J., 2012a. First record and timing of UHP metamorphism from zircon in the Xitieshan terrane: implications for the evolution of the entire North Qaidam metamorphic belt. American Mineralogists 97, 1083–1093.
Liu, F.L., Gerdes, A., Liu, P., 2012b. U–Pb, trace element and Lu–Hf properties of unique dissolution–reprecipitation zircon from UHP eclogite in SW Sulu terrane, eastern China. Gondwana Research 22, 169–183.
Liu, X.C., Wu, Y.B., Gao, S., Wang, H., Zheng, J., Hu, Z., Zhou, L., Yang, S., 2014. Record of multiple stage channelized fluid and melt activities in deeply subducted slab from zircon U–Pb age and Hf–O isotope compositions. Geochimica et Cosmochimica Acta 144, 1–24.
Ludwig, K.R., 2003. ISOPLOT 3.00: A Geochronological Toolkit for Microsoft Excel. Berkeley Geochronology Center, California, Berkeley.
Martin, L.A.J., Duchêne, S., Deloule, E., Vanderhaeghe, O., 2008. Mobility of trace elements and oxygen in zircon during metamorphism: consequences for geochemical tracing. Earth and Planetary Science Letters 267, 161–174.
Mattinson, C.G., Wooden, J.L., Liou, J.G., Bird, D.K., Wu, C.L., 2006. Age and duration of eclogite-facies metamorphism, North Qaidam HP/UHP terrane, Western China. American Journal of Science 306, 683–711.
Morel, M.L.A., Nebel, O., Nebel-Jacobsen, Y.J., Miller, J.S., Vroon, P.Z., 2008. Hafnium isotope characterization of the GJ-1 zircon reference material by solution and laser-ablation MC-ICPMS. Chemical Geology 255, 231–235.
Muehlenbachs, K., 1986. Alteration of the oceanic crust and the ^{18}O history of seawater. In: Valley, J.W., Taylor, H.P., O'Neil, J.R. (Eds.), Stable Isotopes in High Temperature Geological Processes. Reviews in Mineralogy 16, pp. 425–444.
O'Brien, P.J., 2001. Subduction followed by collision: Alpine and Himalayan examples. Physics of the Earth and Planetary Interiors 127, 277–291.
Rubatto, D., 2002. Zircon trace element geochemistry: partitioning with garnet and the link between U–Pb ages and metamorphism. Chemical Geology 184, 123–138.
Rubatto, D., Hermann, J., 2003. Zircon formation during fluid circulation in eclogites (Monviso, Western Alps): implications for Zr and Hf budget in subduction zones. Geochimica et Cosmochimica Acta 67, 2173–2187.
Rubatto, D., Hermann, J., 2007. Zircon behavior in deeply subducted rocks. Elements 3, 31–35.
Rubatto, D., Gebauer, D., Fanning, M., 1998. Jurassic formation and Eocene subduction of the Zermatt–Saas–Fee ophiolites: implications for the geodynamic evolution of the Central and Western Alps. Contributions to Mineralogy and Petrology 132, 269–287.
Rubatto, D., Muntener, O., Barnhoorn, A., Gregory, C., 2008. Dissolution- reprecipitation of zircon at low-temperature, high-pressure conditions (Lanzo Massif, Italy). American Mineralogist 93, 1519–1529.
Rubatto, D., Regis, D., Hermann, J., Boston, K., Engi, M., Beltrando, M., McAlpine, S.R.B., 2011. Yo-yo subduction recorded by accessory minerals in the Italian Western Alps. Nature Geoscience 4, 338–342.
Scherer, E., Munker, C., Mezger, K., 2001. Calibration of the lutetium–hafnium clock. Science 293, 683–687.
Scherer, E.E., Whitehouse, M.J., Munker, C., 2007. Zircon as a monitor of crustal growth. Elements 3, 19–24.
Shi, R., Yang, J.S., Wu, C., Iizuka, T., Hirata, T., 2006. Island arc volcanic rocks in the north Qaidam UHP belt, northern Tibet plateau: evidence for ocean–continent subduction preceding continent–continent subduction. Journal of Asian Earth Sciences 28, 151–159.
Sláma, J., Kosler, J., Condon, D.J., Crowley, J.L., Gerdes, A., Hanchar, J.M., Horstwood, M.S.A., Morris, G.A., Nasdala, L., Norberg, N., Schaltegger, U., Schoene, B., Tubrett, M.N., Whitehouse, M.J., 2008. Plešovice zircon — a new natural reference material for U–Pb and Hf isotopic microanalysis. Chemical Geology 249, 1–35.
Smith, D.C., 1984. Coesite in clinopyroxene in the Caledonides and its implications for geodynamics. Nature 310, 641–644.
Sobolev, N.V., Shatsky, V.S., 1990. Diamond inclusions in garnets from metamorphic rocks: a new environment of diamond formation. Nature 343, 742–746.
Song, S.-G., Yang, J.-S., Liou, J.-G., Wu, C.-L., Shi, R.-D., Xu, Z.-Q., 2003. Petrology, Geochemistry and isotopic ages of eclogites in the Dulan UHPM terrane, the North Qaidam, NW China. Lithos 70, 195–211.
Song, S.-G., Zhang, L.-F., Niu, Y., 2004. Ultra-deep origin of garnet peridotite from the North Qaidam ultrahigh-pressure belt, Northern Tibetan Plateau, NW China. American Mineralogist 89, 1330–1336.
Song, S.-G., Zhang, L.-F., Niu, Y.-L., Su, L., Jian, P., Liu, D.-Y., 2005a. Geochronology of diamond-bearing zircons from garnet peridotite in the North Qaidam UHPM belt Northern Tibetan Plateau: a record of complex histories from oceanic lithosphere subduction to continental collision. Earth and Planetary Science Letters 234, 99–118.
Song, S.G., Zhang, L.F., Chen, J., Liou, J.G., Niu, Y.L., 2005b. Sodic amphibole exsolutions in garnet from garnet-peridotite, North Qaidam UHPM belt, NW China: implications for ultradeep-origin and hydroxyl defects in mantle garnets. American Mineralogist 90, 814–820.
Song, S.G., Zhang, L.F., Niu, Y.L., Su, L., Song, B., Liu, D.Y., 2006. Evolution from oceanic subduction to continental collision: a case study of the Northern Tibetan Plateau inferred from geochemical and geochronological data. Journal of Petrology 47, 435–455.
Song, S.G., Su, L., Li, X.-h, Zhang, G.B., Niu, Y.L., Zhang, L.F., 2010. Tracing the 850-Ma continental flood basalts from a piece of subducted continental crust in the North Qaidam UHPM belt, NW China. Precambrian Research 183, 805–816.
Song, S.G., Su, L., Li, X.H., Niu, Y.L., Zhang, L.F., 2012. Grenville-age orogenesis in the Qaidam–Qilian block: the link between South China and Tarim. Precambrian Research 220–221, 9–22.
Song, S.G., Niu, Y.L., Su, L., Zhang, C., Zhang, L.F., 2014. Continental orogenesis from ocean subduction, continent collision/subduction, to orogen collapse, and orogen recycling: the example of the North Qaidam UHPM belt, NW China. Earth Science Reviews 129, 59–84.
Spandler, C., Hermann, J., Rubatto, D., 2004. Exsolution of thortveitite, yttrialite, and xenotime during low-temperature recrystallization of zircon from New Caledonia, and their significance for trace element incorporation in zircon. American Mineralogist 89, 1795–1806.
Sun, S.-s., McDonough, W.F., 1989. Chemical and isotopic systematics of oceanic basalts: implications for mantle composition and processes. Geological Society Special Publication 42, 313–345.
Tomaschek, F., Kennedy, A.K., Villa, I.M., Lagos, M., Ballhaus, C., 2003. Zircons from Syros, Cyclades, Greece; recrystallization and mobilization of zircon during high pressure metamorphism. Journal of Petrology 44, 1977–2002.
Trail, D., Mojzsis, S.J., Harrison, T.M., Schmitt, A.K., Watson, E.B., Young, E.D., 2007. Constraints on Hadean zircon protoliths from oxygen isotopes, Ti-thermometry, and rate earth elements. Geochemistry, Geophysics, Geosystems 8, 6.
Valley, J.W., Kinny, P.D., Schulze, D.J., Spicuzza, M.J., 1998. Zircon megacrysts from kimberlite: oxygen isotope variability among mantle melts. Contributions to Mineralogy and Petrology 133, 1–11.
Whitehouse, M.J., Platt, J.P., 2003. Dating high-grade metamorphism-constraints from rare-earth elements in zircon and garnet. Contributions to Mineralogy and Petrology 145, 61–74.
Wiedenbeck, M., Alle, P., Corfu, F., Griffin, W.L., Meier, M., Oberli, F., Quadt, A.V., Roddick, J.C., Spiegel, W., 1995. Three natural zircon standards for U–Th–Pb, Lu–Hf, trace element and REE analyses. Geostandards and Geoanalytical Research 19, 1–23.
Woodhead, J.D., Hergt, J.M., 2005. Preliminary appraisal of seven natural zircon reference materials for in situ Hf isotope determination. Geostandards and Geoanalytical Research 29, 183–195.
Wu, Y.-B., Zheng, Y.-F., 2013. Tectonic evolution of a composite collision orogen: an overview on the Qinling–Tongbai–Hong'an–Dabie–Sulu orogenic belt in central China. Gondwana Research 23, 1402–1428.
Wu, F.Y., Yang, Y.H., Xie, L.W., Yang, J.H., Xu, P., 2006a. Hf isotopic compositions of the standard zircons and baddeleyites used in U–Pb geochronology. Chemical Geology 234, 105–126.
Wu, Y.-B., Zheng, Y.-F., Zhao, Z.-F., Gong, B., Liu, X., Wu, F.-Y., 2006b. U–Pb, Hf and O isotope evidence for two episodes of fluid-assisted zircon growth in marble-hosted eclogites from the Dabie orogen. Geochimica et Cosmochimica Acta 70, 3743–3761.
Wu, Y.-B., Hanchar, J.M., Gao, S., Sylvester, P.J., Tubrett, M., Qiu, H.-N., Wijbrans, J.R., Brouwer, F.M., Yang, S.-H., Yang, Q.-J., Liu, Y.-S., Yuan, H.-L., 2009. Age and nature of eclogites in the Huwan shear zone, and the multi-stage evolution of the Qinling–Dabie–Sulu orogen, central China. Earth and Planetary Science Letters 277, 345–354.
Xia, Q.-X., Zheng, Y.-F., Yuan, H.-L., Wu, F.-Y., 2009. Contrasting Lu–Hf and U–Th–Pb isotope systematics between metamorphic growth and recrystallization of zircon from eclogite-facies metagranites in the Dabie orogen, China. Lithos 112, 477–496.
Xia, Q.-X., Zheng, Y.-F., Chen, Y.-X., 2013. Protolith control on fluid availability for zircon growth during continental subduction-zone metamorphism in the Dabie orogen. Journal of Asian Earth Sciences 67–68, 93–113.
Xu, S.T., Okay, A.I., Ji, S.Y., Sengor, A.M.C., Su, W., Liu, Y.C., Jiang, L.L., 1992. Diamond from the Dabie Shan metamorphic rocks and its implication for tectonic setting. Science 256, 80–82.
Xu, P., Wu, F.Y., Xie, L.W., Yang, Y.H., 2004. Hf isotopic compositions of the standard zircons for U–Pb dating. Chinese Science Bulletin 49, 1642–1648.
Yang, J.S., Xu, Z.Q., Zhang, J.X., Song, S.G., Wu, C.L., Shi, R.D., Li, H.B., Brunel, M., 2002. Early Paleozoic North Qaidam UHP metamorphic belt on the northeastern Tibetan plateau and a paired subduction model. Terra Nova 14, 397–404.
Yang, J.S., Wu, C.L., Zhang, J.X., Shi, R.D., Meng, F.C., Wooden, J., Yang, H.-Y., 2006. Protolith of eclogites in the north Qaidam and Altun UHP terrane, NW China: Earlier oceanic crust? Journal of Asian Earth Sciences 28, 185–204.

Yu, S.Y., Zhang, J.X., Li, H.K., Hou, K.J., Mattinson, C.G., Gong, J.H., 2013. Geochemistry, zircon U–Pb geochronology and Lu–Hf isotopic composition of eclogite and their host gneisses in the Dulan area, North Qaidam UHP terrane: new evidence for deep continental subduction. Gondwana Research 23, 901–919.

Zhang, S.-B., Zheng, Y.-F., 2013. Formation and evolution of Precambrian continental lithosphere in South China. Gondwana Research 23, 1241–1260.

Zhang, G.B., Song, S.G., Zhang, L.F., Niu, Y.L., 2008. The subducted oceanic crust within continental-type UHP metamorphic belt in the North Qaidam, NW China: evidence from petrology, geochemistry and geochronology. Lithos 104, 99–118.

Zhang, G.B., Zhang, L.F., Song, S.G., 2009a. UHP metamorphic evolution and SHRIMP geochronologyof a meta-ophiolitic gabbro in the North Qaidam, NW China. Journal of Asian Earth Sciences 35, 310–322.

Zhang, G.B., Ellis, D.J., Christy, A.G., Zhang, L.F., Niu, Y.L., Song, S.G., 2009b. UHP metamorphic evolution of coesite-bearing eclogite from the Yuka terrane, North Qaidam UHPM belt, NW China. European Journal of Mineralogy 21, 1287–1300.

Zhang, J.X., Mattinson, C.G., Yu, S.Y., Li, J.P., Meng, F.C., 2010. U–Pb zircon geochronology of coesite-bearing eclogites from the southern Dulan area of the North Qaidam UHP terrane, northwestern China: spatially and temporally extensive UHP metamorphism during continental subduction. Journal of Metamorphic Geology 28, 955–978.

Zhang, C.-L., Yang, D.-S., Wang, H.-Y., Takahashi, Y., Ye, H.-M., 2011. Neoproterozoic mafic–ultramafic layered intrusion in Quruqtagh of northeastern Tarim Block, NW China: Two phases of mafic igneous activity with different mantle sources. Gondwana Research 19, 177–190.

Zhang, G., Zhang, L., Christy, A.G., 2013a. From oceanic subduction to continental collision: an overview of HP–UHP metamorphic rocks in the North Qaidam UHP belt, NW China. Journal of Asian Earth Sciences 63, 98–111.

Zhang, C., Zhang, L., Bader, T., Song, S., Lou, Y., 2013b. Geochemistry and trace element behaviors of eclogite during its exhumation in the Xitieshan terrane, North Qaidam UHP belt, NW China. Journal of Asian Earth Sciences 63, 81–97.

Zhang, G., Zhang, L., Christy, A.G., Song, S., Li, Q., 2014. Differential exhumation and cooling history of North Qaidam UHP metamorphic rocks, NW China: Constraints from zircon and rutile thermometry and U–Pb geochronology. Lithos 205, 15–27.

Zheng, Y.F., 2009. Fluid regime in continental subduction zones: petrological insights from ultrahigh-pressure metamorphic rocks. Journal of the Geological Society 166, 763–782.

Zheng, Y.-F., 2012. Metamorphic chemical geodynamics in continental subduction zones. Chemical Geology 328, 5–48.

Zheng, Y.-F., Fu, B., Gong, B., Li, Y., 2003. Stable isotope geochemistry of ultrahigh pressure metamorphic rocks from the Dabie–Sulu orogen in China: implications for geodynamics and fluid regime. Earth-Science Reviews 62, 105–161.

Zheng, Y.-F., Wu, Y.-B., Chen, F.K., Gong, B., Li, L., Zhao, Z.-F., 2004. Zircon U–Pb and oxygen isotope evidence for a large-scale ^{18}O depletion event in igneous rocks during the Neoproterozoic. Geochimica et Cosmochimica Acta 68, 4145–4165.

Zheng, Y.-F., Wu, Y.-B., Zhao, Z.-F., Zhang, S.-B., Xu, P., Wu, F.-Y., 2005. Metamorphic effect on zircon Lu–Hf and U–Pb isotope systems in ultrahigh-pressure eclogite-facies metagranite and metabasite. Earth and Planetary Science Letters 240, 378–400.

Zheng, Y.-F., Zhao, Z.-F., Wu, Y.-B., Zhang, S.-B., Liu, X., Wu, F.-Y., 2006. Zircon U–Pb age, Hf and O isotope constraints on protolith origin of ultrahigh-pressure eclogite and gneiss in the Dabie orogen. Chemical Geology 231, 135–158.

Zheng, Y.F., Zhao, Z.F., Chen, Y.X., 2013a. Continental subduction channel processes: Plate interface interaction during continental collision. Chinese Science Bulletin 58, 4371–4377.

Zheng, Y.-F., Xiao, W.-J., Zhao, G.-C., 2013b. Introduction to tectonics of China. Gondwana Research 23, 1189–1206.

Zheng, Y.-F., Chen, Y.-X., Dai, L.-Q., Zhao, Z.-F., 2015. Developing plate tectonics theory from oceanic subduction zones to collisional orogens. Sciences China: Earth Sciences 58, 1045–1069.

Zhou, L.-G., Xia, Q.-X., Zheng, Y.-F., Chen, R.-X., Hu, Z., Yang, Y., 2015. Tectonic evolution from oceanic subduction to continental collision during the closure of Paleotethyan ocean: Geochronological and geochemical constraints from metamorphic rocks in the Hong'an orogen. Gondwana Research 28, 348–370.

Zhu, X.-H., Chen, D.-L., Wang, C., Wang, H., Liu, L., 2015. The initiation, development and termination of the Neoproterozoic-early Paleozoic ocean in the northern margin of Qaidam basin. Acta Geologica Sinca 89, 234–251 (in Chinese with English abstract).